2021•2022

Faculteit Industriële Ingenieurswetenschappen

master in de industriële wetenschappen: nucleaire technologie

Masterthesis

Cycle study of BEAVRS benchmark using different energy deposition models with the OpenMC code

PROMOTOR :

Prof. dr. ir. Gert VAN DEN EYNDE

PROMOTOR :

Dr. Augusto HERNANDEZ SOLIS

COPROMOTOR :

Dr. ir. Luca FIORITO

Liese Boogaerts

Scriptie ingediend tot het behalen van de graad van master in de industriële wetenschappen: nucleaire technologie, afstudeerrichting nucleair en medisch

Gezamenlijke opleiding UHasselt en KU Leuven

2021•2022

Faculteit Industriële Ingenieurswetenschappen

master in de industriële wetenschappen: nucleaire technologie

Masterthesis

Cycle study of BEAVRS benchmark using different energy deposition models with the OpenMC code

PROMOTOR :

Prof. dr. ir. Gert VAN DEN EYNDE

PROMOTOR :

Dr. Augusto HERNANDEZ SOLIS

COPROMOTOR :

Dr. ir. Luca FIORITO

Liese Boogaerts

Scriptie ingediend tot het behalen van de graad van master in de industriële wetenschappen: nucleaire technologie, afstudeerrichting nucleair en medisch

Preface

After studying nuclear for 2.5 years, I wanted a challenge for my master's thesis. I reached out to my professor Prof. Dr. Ir. Gert Van den Eynde and I received a list of several master topics at the SCK CEN. My attention was immediately drawn to this topic that used a new Monte Carlo code. Not long before I had learned about Serpent and practiced basic modelling in Serpent. I already had realized that I liked doing models and simulations. I was really looking forward to expand my knowledge in modelling nuclear reactors and reactor physics. And I can say with certainty that I gained a lot of knowledge during this thesis.

First, I want to thank Prof. Dr. Ir. Gert Van den Eynde to give me the chance to do this topic at the SCK CEN. I am extremely grateful for this opportunity. Second, I cannot begin to express my thanks to Dr. Augusto Hernandez Solis, my mentor at the SCK CEN, who not only guided me through the process, but also wanted to make sure that I understood everything. He would spend hours explaining me reactor physics and would always make time for me to help me. Without him the completion of my thesis would not have been possible.

I am also grateful for my parents. Although they did not understand much about the subject, they always wanted to listen to my explanations about things I did and mistakes I made. They offered their help unconditionally. Special thanks to my boyfriend, who had to listen to my rants about how I solved problems and who I proudly showed my progress. Thank you for listening and supporting.

The resources and services used in this work were provided by the VSC (Flemish Supercomputer Center), funded by the Research Foundation - Flanders (FWO) and the Flemish Government.

Table of contents

List of tables

List of figures

List of abbreviations and definitions

A7	Assembly 7: top right assembly of the BEAVRS core
A97	Assembly 97: central assembly of the BEAVRS core
BEAVRS	Benchmark for Evaluation And Validation of Reactor Simulations
EFPD	Effective Full Power Days
ENDF/B	Evaluated Nuclear Data File/B-version
EOL	End of Life
HFP	Hot Full Power
JRC	Joint Research Centre
PWR	Pressurized Water Reactor
RR	Reaction Rate
SCK CEN	Belgian Nuclear Research Centre

Abstract

Depletion simulations of nuclear systems in Monte Carlo codes use energy deposition models. This thesis investigates the influence of two energy deposition models on three observables of interest, i.e. criticality, the isotopic inventory and fission parameters (i.e. the heating, fission rate and the flux). The first energy deposition model assumes that all energy is deposited locally in the fuel. The other model assumes that photons deposit their energy at the end of their track and that neutrons undergo reactions along their track. The research was performed with the OpenMC-code using a core model from the BEAVRS benchmark. OpenMC is a relatively new, open-source, community-developed Monte Carlo code.

The starting point of the simulations was to keep the core critical at each time-step. The core was depleted for one time-step and after each depletion the critical boron concentration was determined. This concentration was used for depleting the next time-step. With all these values a boron letdown curve was constructed. At each time-step, the isotopic inventory and the fission parameters were also calculated. This procedure was done for both energy deposition models.

One can observe that there is a significant difference between the two energy deposition models. As the second model is assumed as most accurate, the relative error is up to 25% for the isotopic inventory and almost 100% for the criticality. The maximal relative error of the fission parameters is +35% for the top right assembly and -4.5% for the central assembly.

Abstract in het Nederlands

Simulaties van de opbrand van splijtstof in nucleaire systemen met behulp van Monte Carlo codes maken gebruik van energie-depositie-modellen. Deze thesis onderzoekt de invloed van twee energie-depositie-modellen op drie parameters, zijnde de kritikaliteit, de isotopische inventaris en fissie parameters. Het eerste model veronderstelt dat alle energie plaatselijk in de brandstof wordt gedeponeerd. Het tweede model veronderstelt dat fotonen hun energie deponeren aan het einde van hun spoor en dat neutronen reacties ondergaan langs hun spoor. Dit onderzoek is uitgevoerd met de OpenMC-code en een reactorkern uit de BEAVRS *benchmark*. OpenMC is een relatief nieuwe, *open-source*, *community*-ontwikkelde Monte Carlo code.

Het startpunt van de simulaties was om de kern altijd kritisch te houden. De splijtstof werd opgebrand voor één tijdstap en na elke simulatie werd de kritische boorconcentratie bepaald. Dit resultaat werd gebruikt voor de volgende simulatie. Met al deze waardes werd een boordalingscurve opgesteld. Na elke simulatie werden ook de isotopische inventaris en de fissie parameters berekend. Deze procedure werd herhaald voor beide modellen.

Er kan geobserveerd worden dat er een significant verschil is tussen de modellen. Als verondersteld wordt dat het tweede model het meest accuraat is, is het relatieve verschil tot wel 25% voor de isotopische inventaris en bijna 100% voor de kritikaliteit. Het maximale relatieve verschil van de fissie parameters is +35% voor de assemblage rechtsboven en -4.5% voor de centrale assemblage.

1 Introduction

Monte Carlo codes are widely used in the nuclear industry. They can be used for a variety of different applications, for example radiation shielding, radiography and decontamination, among others. There are different types of Monte Carlo codes, some being for instance multi-purpose, while others have been specifically designed for reactor physics applications.

This thesis focuses on multiple observables of interest that come along with the depletion of a pressurized light water reactor core. One of these observables is the criticality of a nuclear system. One way to estimate the criticality is by deterministically solving the neutron transport equation. On the other hand, the Monte Carlo method represents another option to stochastically infer the spatial and spectral distribution of the neutron flux, where the stochastic computation of the neutron population production/losses can be modelled as a matricial system in order to estimate the k-eigenvalue of the system. The k-eigenvalue of the system leads to a conclusion whether the nuclear system is self-sustaining and therefore in a critical state, or not. Because of the nature of the method, the result will come with a statistical uncertainty. To get more accurate results and therefore a smaller uncertainty, more particles and/or histories need to be sampled, which increases the simulation time. This is why the Monte Carlo method is very time-consuming.

Two established Monte Carlo codes that are currently used in the nuclear industry are MCNP [1] and Serpent [2]. MCNP originates from the United States and the first version dates from 1977 [3]. MCNP is a general-purpose code that can be used for neutron, photon, electron, proton or even coupling the transport of such different particles at a time. Examples of applications of MCNP are radiation shielding, medical physics, nuclear criticality safety, decontamination and decommissioning. Both the executable-only distribution package and the distribution package that includes source coding are available on request. To get access to the MCNP packages, the request must be filed and approved. The Radiation Safety Information Computational Centre website (RSICC), based at the Oak Ridge National Laboratory in Oak Ridge, Tennessee, distributes MCNP and states that for non-US citizens generally the executable-only distribution package should be requested [4].

Advantages of MCNP are that it is a well-known and validated code that already proved its worth in the nuclear industry. However, MCNP calculations can be time-consuming due to its programming of handling memory. Thirdly, it can take several months to get the approval for the license.

The second well-known Monte Carlo code is Serpent. As opposed to MNCP, Serpent is a newer Monte Carlo code and is actually born in the reactor physicist community. The first version of Serpent, Serpent 1, dates from 2004, but its development is already discontinued because in 2010 the development of Serpent 2 started. Serpent 1 was originally developed to be a simplified neutron transport code for reactor physics applications, focused on lattice-physics. Serpent 2 however is a fully-oriented reactor physics code, with applications in coupled multi-physics, fusion neutronics and radiation shielding. In addition to the original neutron transport capabilities, Serpent is able to perform photon transport [5] .

Serpent has already proven itself to be faster than MCNP on reactor physics applications. Although it is faster, it uses a large amount of memory. Another disadvantage of Serpent is that is also a license-only code. Thus, this thesis will use the OpenMC-code [6]. OpenMC is a relatively new, community-developed, open-source Monte Carlo code. It has been developed with a focus on running simulations on high-performance computing platforms. It is developed at the Massachusetts Institute of Technology in the United States. OpenMC is capable of performing depletion calculations and is able to track both neutrons and photons.

The primary goal of this master's thesis is to determine the difference between the results of calculations made with different energy deposition models. The starting point of the calculations performed in this research is to keep the core critical during the whole cycle. The primary observable of interest in this thesis is the isotopic inventory at discharge burn-up. Secondly, while depleting the core, the critical boron concentration will be determined at each step. These values are used to construct a boron letdown curve. Also the heating, fission rate and flux for neutrons, photons, electrons and positrons will be calculated. All these observables will be compared for two different energy deposition models. Another aim of this master's thesis is to test the capabilities of a new, open-source, academic code (e.g. OpenMC) in assessing observables of interest.

In a nuclear power plant, energy is mainly generated by the fissions that occur in the reactor fuel. One energy deposition model states that this energy is fully deposited solely in the fuel. It is known that this model is not accurate. The other, more accurate, model that will be explored in this work states that highly energetic photons, referred to as gamma's, travel through the fuel and release their energy in the cladding of the fuel pin or even in the borated water outside the pin. Also the neutron interactions outside the fuel are tracked. These two events cause a redistribution of the energy. The energy deposition in the material is important to determine the burn-up of the material. The energy in the material is linked to the power in the material, which is inevitably linked to the neutron flux in the material. If the neutron flux is over- or underestimated, the burn-up of the materials is also over- or underestimated.

The benchmark that will be used to assess the difference between the two energy deposition models is BEAVRS (Benchmark for Evaluation And Validation of Reactor Simulations) [7]. BEAVRS was proposed in 2013 to serve as a non-proprietary benchmark based on measured reactor data to validate high-fidelity reactor simulations methods. It provides a full-core Pressurized Water Reactor (PWR) depletion model based on two-cycles of operational data from a four-loop Westinghouse-type commercial nuclear power plant [8]. Thus, the benchmark specifications provide not only detailed core and material data so the different participants are able to reproduce their computer models as close to reality as possible, but also provide measured data and scripts for data processing, being these a reliable source of information towards which computer codes can be tested. Therefore, BEAVRS not only represents a good opportunity to assess the OpenMC capabilities of predicting criticality at any point during the bi-cycle study of a full PWR core by means of the boron letdown curve prediction; moreover, it offers the theoretical possibility of studying how the source inventory, computed at each individual assembly, changes due to employment of different energy deposition models during the depletion analysis of a full scale core. This in fact, constitutes the main reason why BEAVRS was chosen as a test case study for this work.

2 Background

2.1 Monte Carlo method

The Monte Carlo method is a stochastic method to obtain a numerical estimate of a deterministic process. This is done by the repeated sampling of random numbers that are used in numerous simulations. These simulations are used to derive the statistical (i.e. average) behaviour of the process [9].

The Monte Carlo method relies on random variables. Random variables are variables whose values depend on the outcome of a random phenomenon. There are two kind of random variables: discrete random variables and continuous random variables. Discrete random variables can only take discrete values. Continuous random variables however can take any value in a certain interval. Both discrete and continuous random variables are described by two functions: the probability density function (PDF) and the cumulative distribution function (CDF). The probability density function is a function that describes the possibility that the sample of the random variable will be a certain value. For a discrete random variable, the probability density function can be a table or a graph, while the probability density function of a continuous random variable is best visualised by a graph. The cumulative distribution function is the probability that the random variable will be a value less than or equal to a certain value. Figure 1 shows an example of a probability density function and a cumulative distribution function of a continuous random variable. Important properties of the PDF and the CDF are that they both cannot be negative, the CDF is always a non-decreasing function of its random variable and the PDF is normalised such that the corresponding CDF varies in the range [0,1].

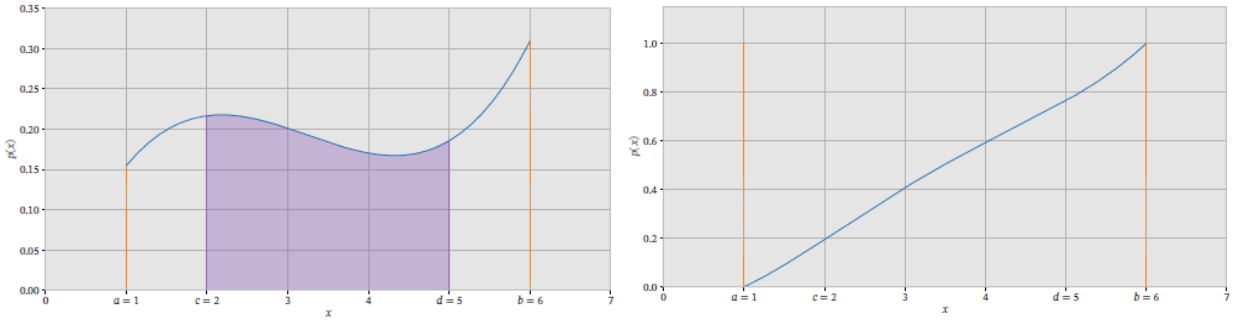

Figure 1: Probability density (left) and cumulative density function (right) of a continuous random variable [9]

The Monte Carlo codes uses random number generators to predict the outcome of a random process. This random process is represented by the PDF and the CDF of that specific process. There are several important factors regarding a random number generator. First, the numbers should be truly random. There should be no bias. Second, the random numbers should be reproducible. Sometimes it is helpful to do the simulations a second time with the exact same input and this is only possible if the same random numbers are used in the simulations. Third, in the end the random numbers will start repeating, but this cannot happen to soon. It is important that the period of the sequence is of great length. Fourth, the random numbers need to be generated and not stored, otherwise there would be a significant amount of memory needed. The last factor is the computer time or the generation time. If a computer is used to generate the random numbers, it should not take a long time generating

them. Same if the numbers are generated by experiment, the experiment should not take too long. As the last factor states, random numbers can be generated using computers or experiments. An example of an experiment is the toss of a coin. But this takes a long time to generate millions of numbers. This is why in modern Monte Carlo codes computers are used to generate the random numbers. But as computer generators are based on an algorithm which is deterministic, they are called pseudo-random generators. This disadvantage does not outweigh the advantages of using computers for generating random numbers, i.e. speed and reproducibility.

As already mentioned, the Monte Carlo method uses numerous simulations to derive the average numerical outcome of the process. The PDF represents a random process and random numbers are sampled to predict the value of the random process. The process develops itself with the acquired value and an outcome is obtained. This procedure repeats itself for multiple simulations and the average is taken of all the outcomes.

2.2 Neutron transport equation

As the previous paragraph states, the Monte Carlo method is used to predict the outcome of a random process. The nuclear phenomenon that is simulated using Monte Carlo codes is the transport of particles, e.g. alpha, beta or gamma particles, neutrons or photons. The transport of particles is a combination of multiple processes. There are several nuclear reactions that can occur if a particle collides with an object made of a certain material. There are two kind of processes: absorption and scattering. When the particles gets absorbed by a nuclei in the material, either capture can occur, or fission can occur. Both of the absorption reactions end in the particle being killed. The two types of scattering reactions are inelastic and elastic scattering, where these reactions do not end the particle. When the particles scatters, it changes its energy but it continues to move on and undergoes new nuclear reactions when it collides. There is no general probability density function that describes the transport of particles, but the PDF's of all the basic processes is known so an estimate is made of the PDF of the combined process.

Some examples of random processes that need to be sampled are: track length, scattering angle and type of reaction. First, the track length or the mean free path is the distance a particle travels before it undergoes a collision. Next, if the particle undergoes a scattering reaction, it gets scattered along a certain angle. Lastly, the type of collision needs to be determined. An easy example is the determination if the collision reaction that occurs is a scattering or an absorption reaction. The macroscopic cross section of absorption is Σ_a and the macroscopic cross section of scattering is Σ_s. Therefore Eq. (1) shows the probability of absorption.

$$\frac{\Sigma_a}{\Sigma_s + \Sigma_a} \tag{1}$$

And Eq. (2) shows the probability of scattering.

$$\frac{\Sigma_s}{\Sigma_s + \Sigma_a} \tag{2}$$

So if a random number η is generated, the following statements can be used to determine whether the reaction is a scattering or an absorption reaction:

$$\eta \leq \frac{\Sigma_a}{\Sigma_s + \Sigma_a} \rightarrow absorption$$

$$\eta > \frac{\Sigma_a}{\Sigma_s + \Sigma_a} \rightarrow scattering$$

Such statements can easily be generalised for more interaction types. The only condition is that all cross sections need to be known.

Figure 2 shows a generic Monte Carlo transport scheme. A particle is created and enters a cell or control volume. First, the mean free path is sampled to the next interaction. Monte Carlo models usually have a geometry that consists of cells that are made of different materials. If the mean free path distance is smaller than the distance to the cell boundary, the particle is moved to the cell boundary and the remaining track length is re-calculated in the new cell. Then if the particle arrives at its destination, the interacting isotope in the material is determined. The isotope is chosen proportional to the total macroscopic cross section for each isotope in the material. If the isotope is chosen, the type of interaction is determined following the procedure described in the previous paragraph. Eventually the interaction resolves and depending on the outcome the particle survives or dies. The particle can die due to the reaction, but it can also end up outside the system. If the particles dies, a new history starts. This procedure is repeated for millions or billions of particles.

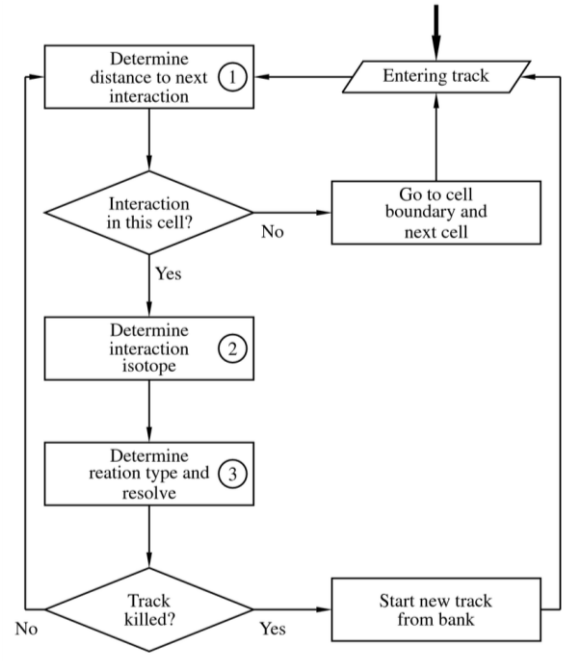

Figure 2: Generic Monte Carlo particle transport scheme [10]

Based on the outcomes of the particle simulations, an estimate is made for the average value and the [1]variance of the quantity of interest. The law of large numbers states that the average of results obtained from a large number of trials should be close to the expected value. If more particle tracks are performed, the average tends to get nearer to the expected value [11]. The Central Limit Theorem states that if a large number of independent random variables are summed up, the normalised sum tends toward a normal distribution even if the originally random variables are not normally distributed. If the sum is normally distributed, the average is also normally distributed. The law of large numbers and the Central Limit Theorem tell us that the variance scales with $\frac{1}{\sqrt{N}}$. This means that in order to largely reduce the variance, a significant number of additional simulations needs to be performed.

2.3 Criticality

In the field of expertise of this master's thesis, i.e. nuclear system physics, the basic quantity of interest that is obtained using the Monte Carlo codes is the criticality of a nuclear system. The nuclear reaction that occurs in the majority of the nuclear systems is fission. Fission splits one heavy nucleus into two lighter ones and when this happens energy is released that can be converted into electricity. The fission reaction has a possibility to occur when a neutron collides with a nucleus. When this happens, typically two to three neutrons are ejected that can again induce fission reactions in other nuclei. Therefore, the fission reaction is a chain reaction. The criticality of a system refers to the way the chain reaction behaves. If a system is critical, the chain reaction is able to sustain itself and the system is therefore self-sustainable. If a system is subcritical, the chain reaction will eventually fade away and when the system is supercritical, the chain reaction will diverge and will eventually become uncontrollable.

The criticality of a system can be assessed using the so-called *k*-eigenvalue problem. The neutron transport equation is a balance equation that equals the gain of neutrons and the loss of neutrons in a certain volume. Equation (3) shows the NTE for a homogeneous problem, meaning that there is no neutron source that is independent of the neutron flux. Equation (4) shows the NTE in operator form. For the system to be critical, the gain and loss in the balance equation should be the same. This is called a stationary problem. The *k*-eigenvalue problem relies on artificially modifying the fission source by a factor k such that the system becomes critical. This is shown by Eq. (5). If the system is supercritical, the actual fission source has to be decreased ($k > 1$). If the system is subcritical, the actual fission source has to be increased ($k < 1$).

[1] The variance is a measure of dispersion, meaning that it is a measure for how far the values are spread out from their average value. The bigger the variance, the more the values differ from the average value and from each other.

$$\frac{1}{v}\frac{\partial}{\partial t}\,\varphi(\boldsymbol{r},E,\hat{\Omega},t)+\ \hat{\Omega}*\ \nabla\varphi(\boldsymbol{r},E,\hat{\Omega},t)+\ \Sigma_t(\boldsymbol{r},E)\varphi(\boldsymbol{r},E,\hat{\Omega},t)$$
$$=\int_0^{4\pi}d\hat{\Omega}'\int_0^{\infty}dE'\,\Sigma_s\left(r,E'\to E,\hat{\Omega}'\to\hat{\Omega}\right)\varphi(\boldsymbol{r},E,\hat{\Omega},t)$$
$$+\ \frac{\mathrm{X}(E)}{4\pi}\int_0^{4\pi}d\hat{\Omega}'\int_0^{\infty}dE'\ \nu(E')\ \Sigma_f(\boldsymbol{r},E',t)\,\varphi(\boldsymbol{r},E',\hat{\Omega}',t)$$

(3)

$$\frac{1}{v}\frac{\delta}{\delta t}\,\varphi(\boldsymbol{r},E,\hat{\Omega},t)+\ \mathcal{M}\varphi(\boldsymbol{r},E,\hat{\Omega},t)=\ \mathcal{F}\varphi(\boldsymbol{r},E,\hat{\Omega},t)$$

(4)

$$\mathcal{M}\varphi(\boldsymbol{r},E,\hat{\Omega},t)=\frac{1}{k}\,\mathcal{F}\varphi(\boldsymbol{r},E,\hat{\Omega},t)$$

(5)

Monte Carlo codes are able to estimate the k-eigenvalue. When the Monte Carlo code gives back this value, it tells the nuclear physicists more about the state of the nuclear system. If the *k*-eigenvalue is not equal to 1, adaptions can be made to the utilised materials and to the geometry to make sure the nuclear system is critical.

2.4 Depletion

Depletion simulations predict the time-evolution of the isotopic composition of the nuclear fuel. During operation, the materials present in a nuclear power plant transmute due to reactions. This is called burn-up. Burn-up involves both production and loss of isotopes. For example, fission reactions transform heavy nuclides in lighter fission products. Actinides, fission products, etc. can absorb neutrons and transform into other isotopes. They will also decay according to their half-lives. All these processes combined is called depletion. These simulations are important because reactor parameters and Spent Nuclear Fuel (SNF) parameters depend on burn-up. Reactor parameters are for example reactor reactivity and the neutron flux. Relevant parameters for SNF are decay heat, neutron and γ emission and radiotoxicity. Burn-up is used as a measure for the total energy that is produced by the nuclear fuel during the operation of the reactor. It is also an indicator for the grade of use of the nuclear fuel. Burn-up is commonly expressed in terms of energy released up to now per ton of heavy metal initially present (MW d/t_{HM}).

The mathematical model of depletion is called the Bateman equation. The starting general equation is shown in Eq. (6).

$$\frac{d}{dt}N_i(t)=production\ of\ N_i-loss\ of\ N_i$$

(6)

Production processes are decay from isotope j to isotope i, neutron reactions from isotope j to isotope i and fission that creates different fission products. Loss is caused by the decay of isotope i and neutron absorption in an isotope. The general equation for an isotope 'i' is given in Eq. (7).

$$\frac{d}{dt}N_i(t) = \sum_{j \neq i}\left\{\lambda_{j\to i} + \int_0^\infty \sigma_{j\to i}(E)\,\phi(E)\,dE + \int_0^\infty \gamma_{j\to i}\sigma_{f,j}(E)\,\phi(E)\,dE\right\} N_j(t)$$

$$-\left\{\lambda_i + \int_0^\infty \sigma_{a,i}(E)\,\phi(E)\,dE\right\} N_i(t)$$

(7)

Equation (7) can also be written in matrix form for all isotopes considered in a system. This is shown in Eq. (8). The matrix **A** is called the transition matrix.

$$\frac{d}{dt}\boldsymbol{N}(t) = \boldsymbol{A}(t)\,\boldsymbol{N}(t); \boldsymbol{N}(t_o) = \boldsymbol{N}_0$$

(8)

Equation (8) represents a coupled set of ordinary differential equation which, depending on the number of isotopes considered, can be of large size. It is almost not possible to solve this set analytically. The simplest numerical method to solve Eq. (8) is known as the 'predictor' method. This method divides the overall time interval of interest into smaller time-steps. If the transition matrix **A** is considered to be constant in a time-step, the linear system of ordinary differential equations can be analytically written as Eq. (9) in such time-step.

$$\boldsymbol{N}(t) = e^{\boldsymbol{A}(t-t_0)}\boldsymbol{N}(t_0)\ with\ e^{\boldsymbol{A}t} = \sum_{k=0}^{\infty}\frac{1}{k!}(\boldsymbol{A}t)^k$$

(9)

The matrix exponential e^{At} needs an approximation and this can be achieved with the 'Chebyshev Rational Approximation Method (CRAM)'. Higher-order CRAM can be used to solve the Bateman equation accurately for time-steps of the order of 1 million years [12].

2.5 Energy deposition models

Energy depletion models are very important while depleting at constant power. The power produced in the depleting material dictates the real flux level at which the reactions will take place. This information is required to solve the Bateman equation. The original, and default model in Monte Carlo codes, energy deposition model assumes that all energy is deposited locally in the fuel. This results in an overestimation of the power generated in the material, leading to an overestimation of the normalisation factor which leads to an overestimation of the fission reaction rate. If the overestimated fission RR is used to solve the Bateman equation, the burn-up will also be overestimated. This can lead to significant differences in the isotopic inventory at EOL. If for example the SNF is transported to an intermediate storage and there is actually a larger amount of fissile material left in the SNF than the calculations estimated, this can lead to safety issues.

The Serpent development team [13] states that Serpent 2 has four different energy deposition models. OpenMC is based on Serpent and uses the same methodology for the energy deposition models. In Serpent 2, the user can specify which energy deposition model the code must use during the simulation by means of the EDEP input card.

2.5.1 EDEP mode 0

EDEP mode 0 is the default mode used in the simulations of both OpenMC and Serpent 2. It assumes that all energy is deposited locally in the fuel. To determine the energy deposition per nuclide the Q-value of that specific nuclide is used in the calculation. The Q-value is the amount of energy that is released or absorbed during a reaction.

2.5.2 EDEP mode 1

EDEP mode 1 is similar to EDEP mode 0. It also assumes local energy deposition, but the energy deposition per fission is calculated based on Q-values taken by MF = 1 MT = 458 data. This data consists of Q-values due to fission as a function of incident neutron energy. This means that there is a distinction between the different Q-values from fission reactions depending on the energy of the incident neutron, as opposed to EDEP mode 1 were it was just one lumped Q-value.

2.5.3 EDEP mode 2

EDEP mode 2 is a significant improvement compared to the previous modes. It allows the fission neutrons to deposit their energy along their track as they undergo interactions. This way the neutrons can deposit their energy outside the fuel, for example in the cladding or in the borated water. This leads to a redistribution of energy due to the neutron interactions. Energy release due to reactions other than fissions is calculated using KERMA factors. The photons that are released during the fissions still deposit their energy at the fission reaction sites in the fuel.

2.5.4 EDEP mode 3

EDEP mode 3 is the most accurate model of energy deposition. It involves a coupled neutron-photon transport calculation. Similar to EDEP mode 2, the deposition of the neutron energy is tracked along its history of reactions. The improvement over mode 2 is in treatment of gammas. The photons that are emitted during the reactions travel to their final destination and deposit their energy. Photon energy deposition is calculated using a tally which is scored after each energy loss interaction: photoelectric effect, Compton scattering and pair production. This leads to a redistribution of the energy. In conclusion, EDEP mode 3 takes all three factors in account: the energy due to fissions, the neutron KERMA and the photon transport and energy deposition.

3 Methodology

3.1 Material

OpenMC is a community-developed, open-source Monte Carlo code. It is able to track both neutrons and photons and is capable of performing fixed source, k-eigenvalue, and subcritical multiplication calculations on models. These models can be build using a constructive solid geometry or a CAD representation. OpenMC is able to run in parallel using a hybrid MPI and OpenMP programming model. It has been extensively tested on leadership class supercomputers [14].

The OpenMC team [14] explains more about the code in detail: "One of the unique features of OpenMC is its rich, extensible Python and C/C++ programming interfaces that enable programming pre- and post-processing, multigroup cross section generation, workflow automation, depletion calculations, multiphysics coupling, and the visualization of geometry and tally results. In addition to the core Monte Carlo transport solver and associated APIs, OpenMC includes a Python-based nuclear data interface that enables power users to inspect, modify, and perform various types of nuclear data processing on ENDF, ACE, and OpenMC's native HDF5 files. To ensure the quality and accuracy of the code over time, a supporting infrastructure has been developed that includes continuous integration testing and automated critical benchmark simulations, cross-code comparisons, and performance testing.".

The Flemish Supercomputer Center (Vlaams Supercomputer Centrum - VSC) is a partnership between the five Flemish universities and their university associations: Associatie Universiteit & Hogescholen Antwerpen, Universitaire Associatie Brussel, Associatie Universiteit Gent, Associatie KU Leuven and Associatie Universiteit-Hogescholen Limburg [15]. The VSC possesses a Tier-1 and Tier-2 infrastructure [16]. As a student of a Flemish University, access is granted to the Tier-2 infrastructure. For this work, the VSC supercomputer was used to run the simulations.

In order to explore the impact of the different energy deposition models, a representative depletion benchmark needed to be selected. This thesis uses the BEAVRS benchmark [7]. BEAVRS stands for 'Benchmark for Evaluation And Validation of Reactor Simulations' and it represents a 4-loop Westinghouse pressurized water reactor. It contains three different fuel enrichments of UO_2 in the first cycle: 1.6%, 2.4% and 3.1%. The core consists of 193 fuel assemblies and each fuel assembly consists of 17x17 rods. 264 of these rods are fuel rods, the other 25 pins are instrument tubes, burnable poison rods, control rods or guide tubes.

3.2 Method

First, the BEAVRS model will be built in 3D using constructive solid geometry. A transport calculation will be performed to confirm that the BEAVRS core is in fact critical. This calculation will be done under cold conditions, i.e. a temperature of 566.48 K and a boron concentration of 975 ppm. After the criticality confirmation the model will be updated to Hot Full Power conditions (HFP) and a critical boron concentration search will be performed. The HFP condition implies of a temperature of the fuel of 900 K and a temperature of all other materials of 600 K. The HFP obtained critical concentration will be used for the first depletion step. Table 1 shows the depletion steps, as prescribed in BEAVRS. It shows a cumulative procedure. This means that the first depletion step will go from 0 EFPD to 4 EFPD and the second step goes from 4 EFPD to 11 EFPD, and so on.

Table 1: EFPD - depletion steps

0	4	11	16	22	31	36	52
69	85	124	185	177	204	214	219

After each depletion step, a critical boron concentration search will be performed. This concentration will be used in the next depletion step. A depletion consists of two transport calculations. This means that if the boron concentration gets adjusted each step, the first transport calculation will always be critical. The process of searching and depleting will be repeated until the boron concentration hits zero. Using all such obtained critical boron concentrations, a boron letdown curve will be constructed.

Simultaneously with the gradual construction of the boron letdown curve, the evolution of several nuclides in time will be tracked. The nuclides of interest are: Cm-244, Eu-154, Am-241, Nd-148, Cs-137, Y-90, Sr-90, Pu-239, Pu-240, Pu-241, Xe-135, Sm-149, U-235 and U-238. The choice of these is explained in 3.3. The atom density of the isotopes will be researched in function of the EFPD (Effective Full Power Days).

At each depletion step the heating, fission rate and flux will be calculated. OpenMC has a specific class for this purpose, similar to Serpent and MCNP. The *openmc.Tally* estimates the physical quantities in the simulations, such as the flux, the total reaction rate and the total scattering rate, but also very specific quantities like the (n,2n) reaction rate. As a tally estimates the scoring function that is integrated over energy and space, i.e. over a particular region of the phase space, filters need to be specified. There are several options to define such phase space region. The most used options are the cell filter, the material filter and the energy filter. As the names already suggest, they specify in which cell, material and at what energies the events should score to the tally. In this thesis, the heating, fission rate and flux will be calculated at the central assembly (assembly 97) and the upper right assembly (assembly 7). The results of the two assemblies will be compared between the different energy deposition models. The heating and flux will be calculated for neutrons, and in the case of the second energy deposition model, also for photons, electrons and positrons.

This procedure of constructing a boron letdown curve, isotopic inventory graph and tallying will be repeated for the two different energy deposition models. These two models will be evaluated and compared to each other to determine whether the energy deposition has an influence on the criticality, the isotopic inventory and the fission parameters.

3.3 Choice of isotopes

The isotopic inventory research consists of 14 isotopes: Cm-244, Eu-154, Am-241, Nd-148, Cs-137, Y-90, Sr-90, Pu-239, Pu-240, Pu-241, Xe-135, Sm-149, U-235 and U-238. The choice of these nuclides is based on their behaviour inside the fuel during operation of the PWR and on their behaviour outside during transport, intermediate storage and final disposal.

The first nuclides that are chosen are fissile isotopes and neutron poisons that will strongly influence the reactivity. Both Xe-135 and Sm-149 are neutron poisons. These isotopes have a very large cross section for neutron absorption. This causes a decrease of the reactivity, because less neutrons mean less fissions. The nuclide Sm-149 is not a fission product, but is a daughter of Nd-149. The radionuclide Nd-149 is a fission product and a beta-emitter. It decays to Pm-149 with a half-life of 1.7h and in its turn Pm-149 decays to Sm-149 with a half-life of 53h. Because the half-life of Nd-149 (1.7h) is much less than the half-life of Pm-149 (53h), Sm-149 is considered a daughter of Nd-149. The nuclide Sm-149 is stable and only disappears due to neutron capture, with a neutron absorption cross section of about 56 000 barn.

The nuclide Xe-135 is a fission product, but it can also be created by radioactive decay. The radionuclide I-135 decays to Xe-135 and is created by decay of Te-135 or as a direct fission product. Also Te-135 itself is created as a direct fission product. As the decay from Te-135 to I-135 happens really fast ($T_{1/2}$ = 18.6 s), Xe-135 is considered a daughter of I-135. As opposed to Sm-19, Xe-135 is not stable and undergoes beta decay to Cs-135 with a half-life of 9,1h. It also disappears by neutron absorption to Xe-136, which is stable. The neutron absorption cross section of Xe-135 is about 2 650 000 barn. Both Sm-149 and Xe-135 will reach an equilibrium during operation. This equilibrium level is independent of the flux for Sm-149, but dependent for Xe-135.

The next chosen isotopes are the original isotopes in the fuel, such as U-235 and U-238. The former, U-235, is the main fissile isotope and it will gradually decrease due to fissions and other transmutations. The latter, U-238, is more prone to neutron absorption and will transmute to U-239. This is follow by the decay of U-239 to Pu-239 by two β^--decays. The nuclide Pu-239 is an isotope that is commonly used as fuel in nuclear reactors and in nuclear weapons. The important property of Pu-239 is that its critical mass (= 10 kg) is much smaller than the critical mass of U-235 (= 52 kg). When Pu-239 captures a neutron, Pu-240 is created. An important property of Pu-240 is that its secondary decay way is spontaneous fission. It transmutes to Pu-241 by neutron capture. The nuclide Pu-241 is fissile with a neutron absorption cross section larger than the neutron absorption cross section of Pu-239, respectively 1010 barn and 752 barn [17]. They both have a similar ratio of neutron fission over absorption cross section, with neutron absorption cross sections of respectively 370 barn and 270 barn [17]. Most importantly, the inventory of fissile nuclides and fission products with large neutron absorption cross sections is used for criticality safety during transport, storage and disposal.

The remaining isotopes are important during transport, intermediate storage and final disposal. The main observables of interest that influence the safety and the ecological and economical aspect of transport, storage and disposal are decay heat and neutron and γ-ray emission rate. Decay heat originates from the decay of radionuclides present in the fuel. The different radionuclides that are present in the fuel have a broad range of half-lives. This causes that the fuel has to be cooled for a long time. The research of observables of interest for SNF [18] states that Sr-90, Y-90, Cs-137, Am-241 and Cm-244 are important to assess the decay heat. The nuclide Sr-90 decays to Y-90 by

β-decay. The second observable is the neutron emission rate. Neutron emissions happen due to spontaneous fission reactions and (α,n) reactions. The first type of reaction occurs dominantly in heavy nuclides, mostly Cm-244. As previously mentioned, Pu-240 also contributes to the neutron emissions with spontaneous fission, but on a significantly lower level. The contribution of (α,n) reactions is mainly due to the α-decay of Pu-239, Pu-240, Cm-244 and Am-241. The last observable is the γ-ray emission rate. The γ-ray emissions are dominated by the decays of the fission products and therefore Eu-154 is chosen.

In addition to these observables, fission products can also be used as indicators for burn-up and power. The research of observables of interest of SNF [18] explains that Nd-148 is often used a burnup indicator. It is produced by neutron induced fission or by decay of very short living fission products ($T_{1/2}$ < 2 min). The production rate of Nd-148 nuclei is proportional to the total fission rate. The half-life of Nd-148 is 3 x 10^{18} year and is therefore considered stable. This means that the loss of Nd-148 is negligible. The nuclide Sm-149 is chosen as a power indicator. As already explained, Sm-149 is a neutron poison that reaches an equilibrium that is independent on the flux. The equilibrium concentration however is in function of the fission rate, which is assumed to be proportional to the reactor power. When the power changes, the equilibrium concentration of Sm-149 reaches a different level. The nuclide Sm-149 is stable and after the decay of all the Pm-149 nuclei, its concentration is independent of the cooling time.

4 BEAVRS 3D-model

4.1 Model

The BEAVRS 3D-model was built using constructive solid geometry based on the benchmark document [7]. The BEAVRS core consists of 193 assemblies. Each assembly is made of a square lattice of 17 x 17 rods, i.e. 289 rods. As already mentioned, 264 of these rods are fuel rods. The remaining places are filled with control rods, instrument tubes, empty guide tubes or burnable poison rods. The location and number of the latter are dependent on the fuel assembly position in the core.

The following figures are plots generated by OpenMC.

Figure 3 shows the axial view of the BEAVRS core at z = 230 cm. The full height of the core is 460 cm. The core consists of three different enrichments of UO_2. Purple represents 3.1% enrichment, yellow 2.4% enrichment and light pink 1.6% enrichment.

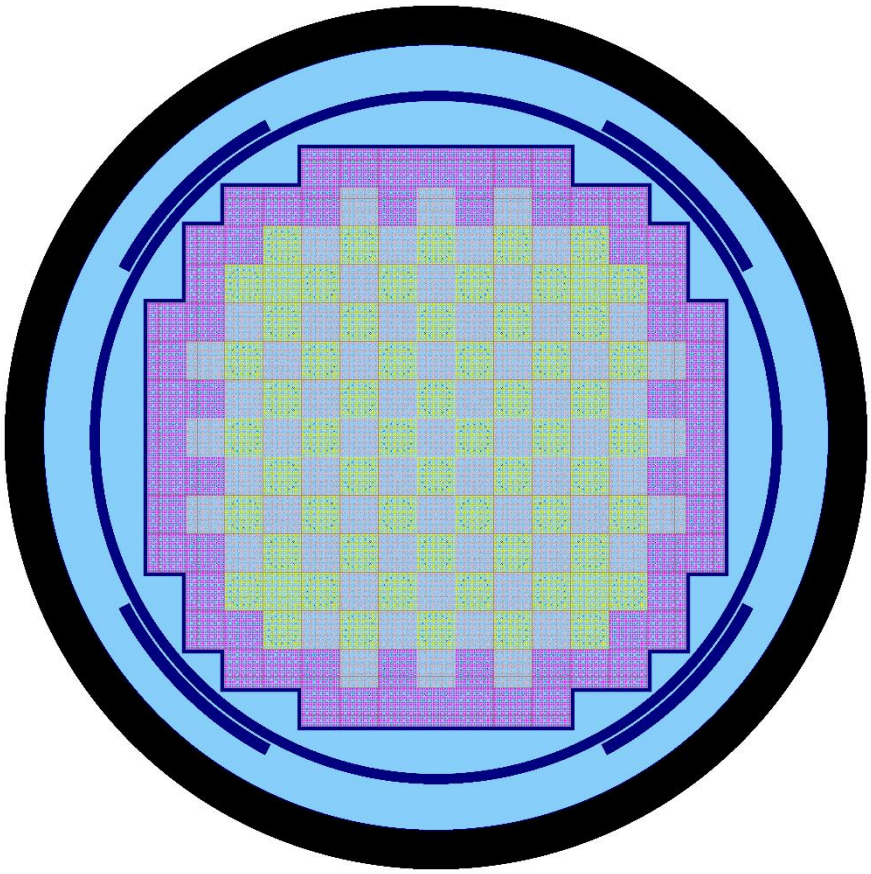

Figure 3: Radial view of the BEAVRS core at z = 230 cm

To optimise depletion and post-processing, every assembly is treated as a different material. This is shown in Figure 4. This method of modelling the core is chosen because the depletion of the material depends on the location of the assembly in the core.

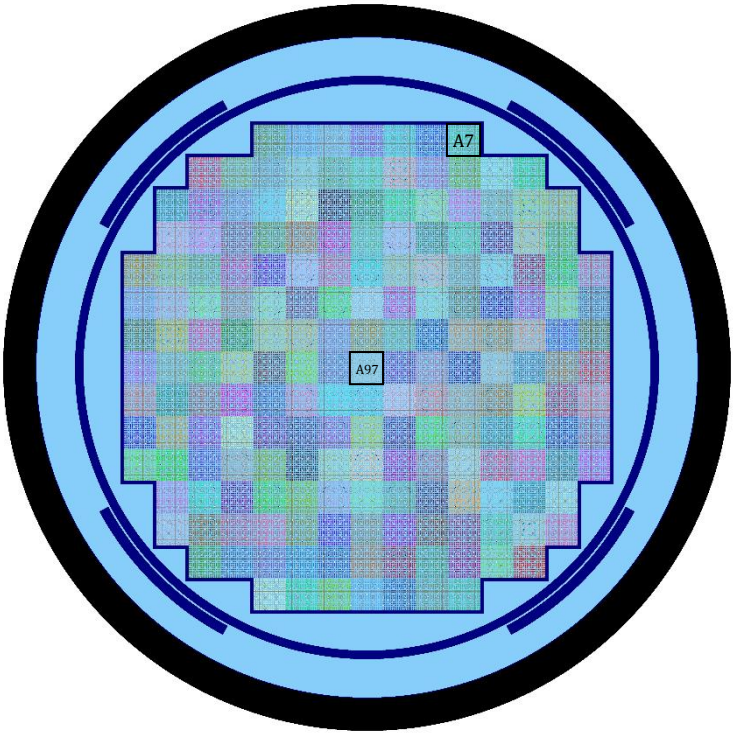

Figure 4: Radial view of the BEAVRS core at z = 230 cm, with colours representing every assembly material

The fission parameters, i.e. flux, fission rate and heating, are evaluated in two assemblies. The chosen assemblies are indicated on Figure 4.

Figure 5 shows assembly 7, referred to as A7. Assembly 7 is the top right assembly of the core. It consists of fuel rods of 3.1% enrichment and no burnable poison rods or control rods. There is also no central instrument tube present. The dedicated fuel-free locations are filled with guide tubes.

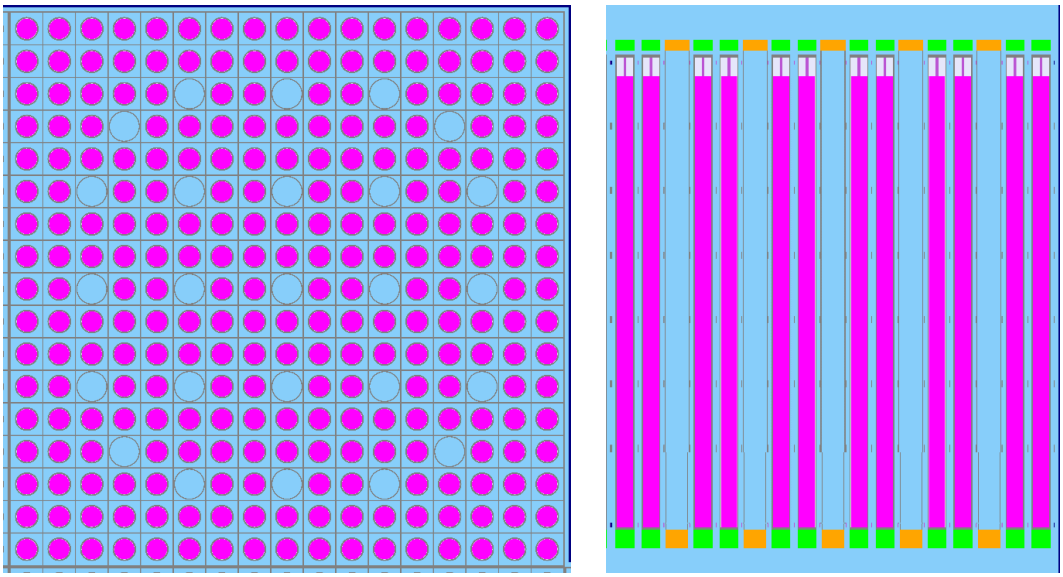

Figure 5: Radial view at z = 230 cm (left) and axial view (right) of A7

Figure 6 shows assembly 97, referred to as A97. Assembly 97 is the central assembly of the core. It consists of fuel rods of 1.6% enrichment and no burnable poison rods. The central pin is a guide tube and the other locations are reserved for control rods. As the depletion happens at full power, the control rods are completely withdrawn. The control rods are made of two materials: the bottom part of the control rod is made of Ag-In-Cd and the upper region is made of boron carbide (B_4C). The Ag-In-Cd alloy is composed of 80% Ag, 15% In and 5% Cd.

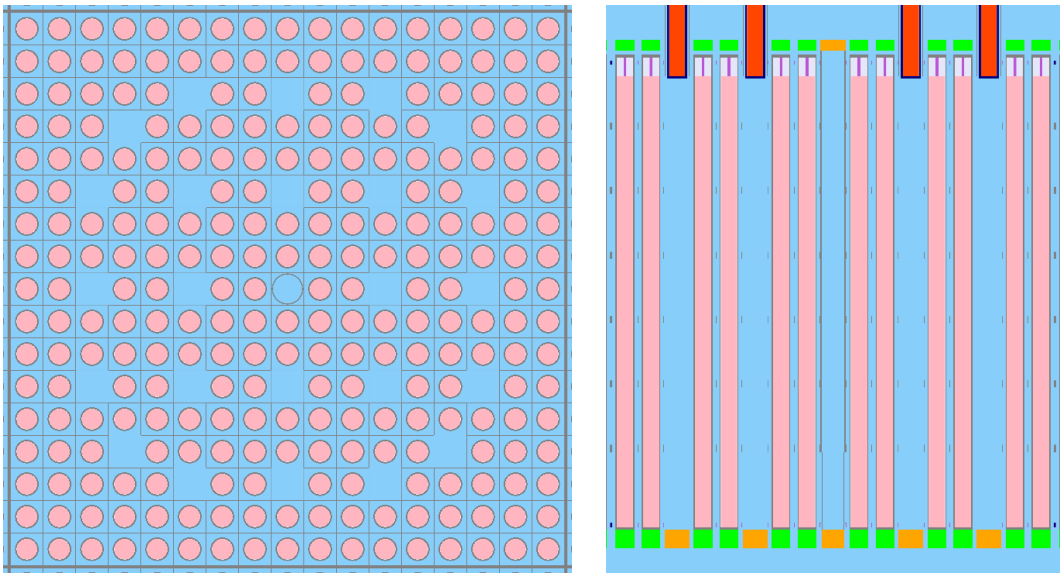

Figure 6: Radial view at z = 230 cm (left) and axial view (right) of A97

4.2 Transport

After extensive geometry debugging of the core, the first transport calculation was performed to assure the core was in fact critical. The core was updated to cold conditions, meaning that the temperature of the whole core was set to 560 °F (= 293,33 °C) and the boron concentration in the borated water was set to 975 ppm.

Two different cross section libraries were used in the simulations to determine which one would be the most accurate: ENDF/B-VIII.0 and JEFF 3.3 were evaluated. A third option, ENDF/B-VII.1 was not evaluated because several isotopes that were present in BEAVRS were not available in the data library. Table 2 shows the results of the calculations using ENDF/B-VIII.0 and JEFF 3.3. All simulations were performed using 350 active cycles, 50 inactive cycles and 100 000 particles.

Table 2: Results transport calculation using different data libraries

	k-eff	uncertainty
ENDF/B-VIII.0	1.00170	0.00017
JEFF 3.3	1.00470	0.00016

These results show that the BEAVRS core is in fact close to critical. It was decided to use the ENDF/B-VIII.0 library for the following research. These calculations already proved that OpenMC is capable of assessing the criticality with a relative small uncertainty with a not particular high number of cycles and/or particles.

5 Boron letdown curve

The starting point of this research was to keep the core critical during each depletion step. To achieve this, the depleted materials will be analysed after each time-step and a new boron concentration will be determined. Then the new critical boron concentration was used in the next depletion step. All depletion calculations were performed with 300 active cycles, 50 inactive cycles and 100 000 particles. The depletion chain that was used is the CASL-U-2015-2014-000, Rev. 0, ORNL/TM2016/53,2016. All depletions are performed using the predictor method and CRAM48. With these specifications, the uncertainty on the k-eff lies within a range of 0.00014 to 0.00017.

The critical boron search was performed using a build-in function of OpenMC, i.e. *openmc.search_for_keff()*. This function requires a second function that creates a parametrised model to analyse. This second function returns a model of the core with the boron concentration as parameter. The search function itself has several arguments that can be passed, for example an initial guess of the critical boron concentration, a bracketed range for the expected critical boron concentration, the tolerance and the method. The search function picks a value for the boron concentration and runs a transport calculation to determine the k-eff. According to this result, the function alters the value of the boron concentration and re-runs the transport calculation. When it is finished, it returns a list of guesses and corresponding k-eff values and ends with the final result.

For all search calculations 900 active cycles, 100 inactive cycles and 10 000 particles were used. The tolerance for the search function was set to 1E-4.

Table 3 shows the simulation times for depletion for both energy deposition modes. The simulation time for one step for EDEP mode 0 takes on average almost 62 minutes, for EDEP mode 3 this is 225 minutes. The total simulation time for EDEP mode 0 is 865 minutes, e.g. 14 hours and 26 minutes. This is just a fraction of the total simulation time of EDEP mode 3 that has a total duration of 3151 minutes, e.g. 52 hours and 31 minutes. EDEP mode 3 needs more than 3.5 times more time than EDEP mode 0.

Table 3: Depletion simulation times for EDEP mode 0 and EDEP mode 3

depletion steps [EFPD]	EDEP mode 0 [minutes]	EDEP mode 3 [minutes]
0 - 4	63	232
4 - 11	65	217
11 - 16	62	230
16 - 22	61	228
22 - 31	60	222
31 - 36	60	218
36 - 52	66	245
52 - 69	62	216
69 - 85	60	228
85 - 124	59	218
124 - 152	60	232
152 - 177	60	220
177 - 204	64	228
204 - 219	63	217
average	61.79	225.07
total	865	3151

5.1 Boron letdown curve of EDEP mode 0

Table 4 shows the search results for EDEP mode 0 and Figure 7 shows the line chart of the critical boron concentration in function of the EFPD.

There is a significant increase in simulation time between 0 EFPD and 4 EFPD. This is caused by the increase in material complexity due to depletion. The last search step does not have a simulation time because the search function did not succeed. For the last step, the bracketed range was set from 0 to 30. When the search function performed the transport calculation with 0 ppm, it obtained a subcritical core. As the boron concentration cannot go below zero, the search stopped. This means that the core actually reached a critical boron concentration of 0 ppm before 214 EFPD.

Table 4: Critical boron search results - EDEP mode 0

EFPD	Critical boron concentration [ppm]	Simulation time [min]
0	919	32
4	651	89
11	621	88
16	613	87
22	608	82
31	595	79
36	588	78
52	548	86
69	502	77
85	448	82
124	311	90
152	213	94
177	123	95
204	30	100
214	0	

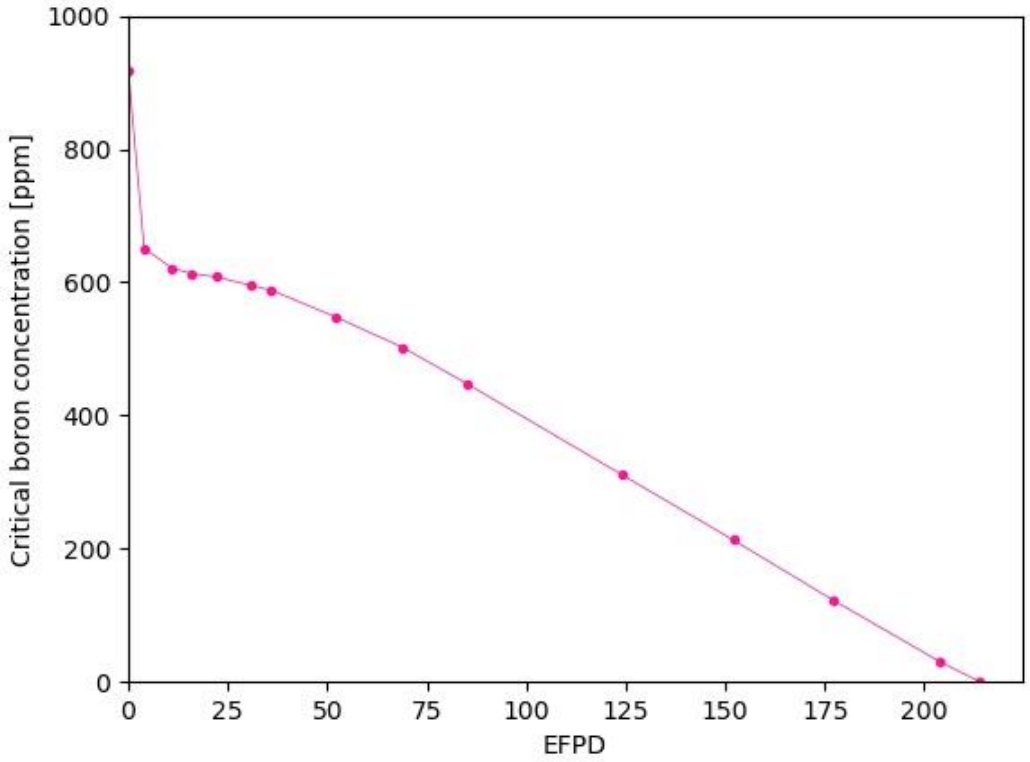

Figure 7: Boron letdown curve - EDEP mode 0

To obtain an impression of the EFPD at which the critical boron concentration hits zero ppm, a linear regression was performed on the data from 69 EFPD to 204 EFPD. Between these values, a linear decrease of the critical boron concentration is shown. Eq. (10) shows the results of the linear regression.

$$y = -3{,}507197x + 745{,}222769 \tag{10}$$

To get an estimation of the EFPD where the critical boron concentration hits zero, this equation is solved for y = 0. The result is 212.48 EFPD.

5.2 Boron letdown curve of EDEP mode 3

Table 5 shows the results for EDEP mode 3 and Figure 8 shows the line chart of the critical boron concentration in function of the EFPD.

As already mentioned, the search function uses a second function that builds a model of the core under analysis. For EDEP mode 3, one alteration had to be made on the model of EDEP mode 0. The geometry and the materials are the same, but for EDEP mode 3 photon transport had to be activated. This caused the simulations to be significantly longer. The jump in simulation time between 0 EFPD and 4 EFPD is for the same reason as with the results from EDEP mode 0. The material complexity of the fuel increases significantly after the first depletion step. Similar to EDEP mode 0, the last search function did not succeed.

Table 5: Critical boron search results - EDEP mode 3

EFPD	Critical boron concentration [ppm]	Simulation time [min]
0	914	80
4	654	377
11	623	370
16	614	382
22	610	371
31	597	366
36	590	322
52	555	342
69	512	374
85	462	341
124	332	391
152	235	394
177	151	391
204	67	444
214	26	473
219	0	

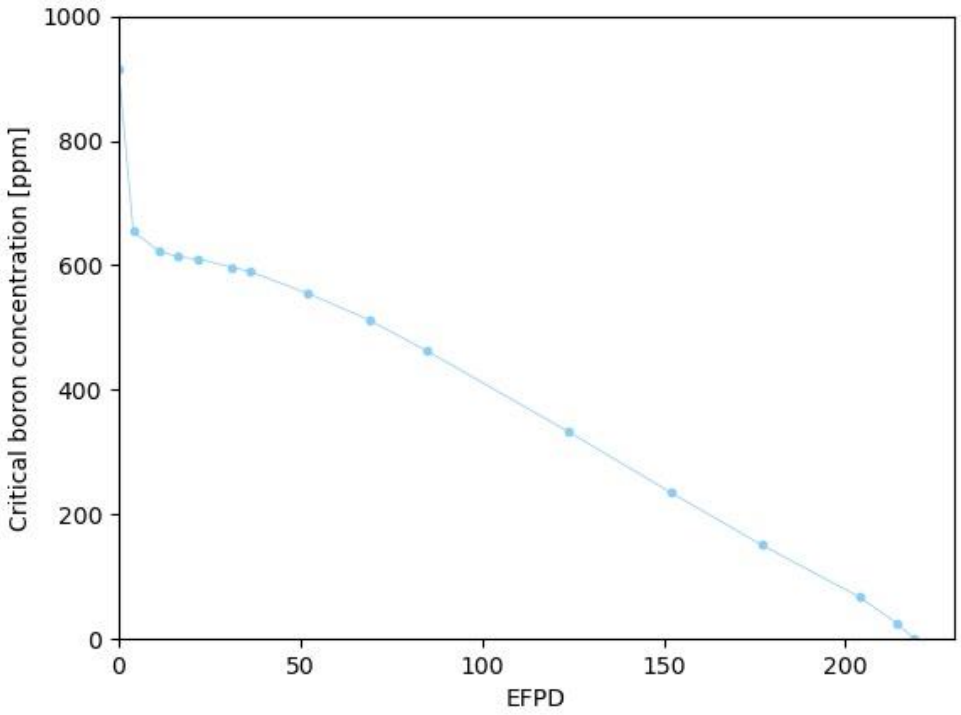

Figure 8: Boron letdown curve - EDEP mode 3

The same procedure as EDEP mode 0 was followed to obtain an impression of the EFPD at which the critical boron concentration would hit zero ppm. The linear regression was carried out on the data from 69 EFPD to 214 EFPD. Eq. (11) shows the result of the linear regression.

$$y = -3{,}344019x + 744{,}659927 \tag{11}$$

To get an estimation of the EFPD where the critical boron concentration would reach zero, this equation is solved for y = 0. The result is 222.68 EFPD. It was expected that the result would be smaller than 219 EFPD. But it is shown in the chart that the last step deviates from the linear decrease. This explains why the result from the linear regression is higher. The failure of the last search function can be explained by the nature of the Monte Carlo method. The result of the search function for a boron concentration of 0 ppm was a k-eff = 0.99993 with an uncertainty of 0.00028. The critical core of k-eff = 1 lies within the range of the uncertainty. If the simulation was performed with more cycles or particles, the uncertainty would be lower and criticality would maybe be reached. It is expected that if this simulation will be performed, the core should be critical or supercritical with 0 ppm at 219 EFPD. This simulation is not performed as the simulation time would be extremely long and the result would have no added value for this research.

5.3 Comparison between EDEP mode 0 and EDEP mode 3

Figure 9 shows the boron letdown curves of EDEP mode 0 and EDEP mode 3 together. There can be concluded that the further the depletion progresses, the more significant the difference is between the two modes. The results show that EDEP mode 0 underestimates the critical boron concentration. This phenomena can be explained by the burn-up of the fuel. As already explained, EDEP mode 0 assumes that all the energy is deposited locally. This causes an overestimation of the power in the fuel and therefore an overestimation of the fission reaction rate. This heavily influences the solution of the Bateman equation. As the fission RR is overestimated, more burn-up will occur in the fuel and therefore the core will become less critical. This is why the critical boron concentration is lower for EDEP mode 0. A lower concentration of boron is needed to make the core critical because there is a smaller amount of fissile material present. Figure 10 shows the relative error between the two modes. At the end of the cycle, the error becomes extremely significant.

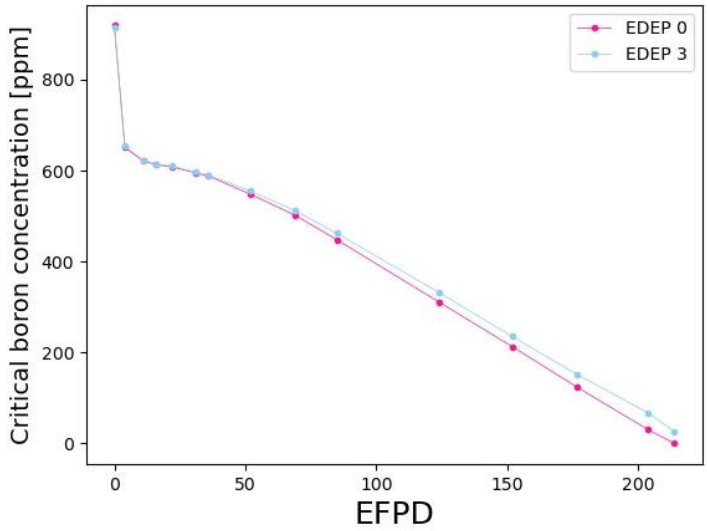

Figure 9: Boron letdown curves for EDEP 0 and EDEP 3

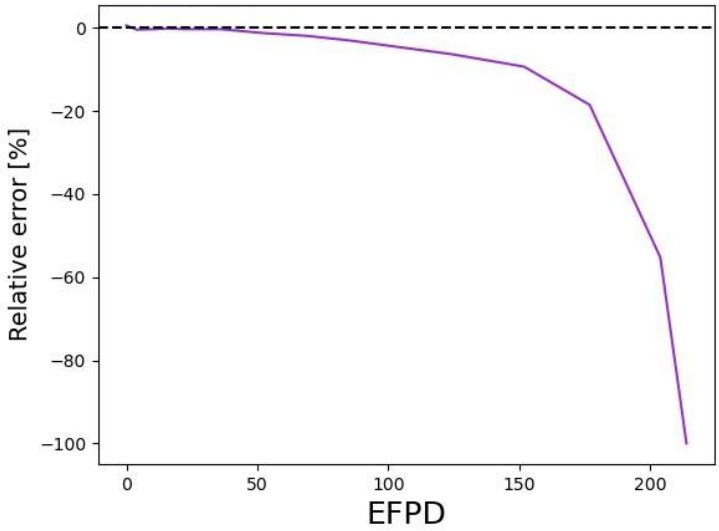

Figure 10: Relative error between critical boron concentrations of EDEP 0 and EDEP 3

6 Isotopic inventory

This chapter will describe the results from the isotopic inventory calculations. After each depletion step, the atom density of 14 isotopes is determined. The isotopes that are evaluated are: Cm-244, Eu-154, Am-241, Nd-148, Cs-137, Y-90, Sr-90, Pu-239, Pu-240, Pu-241, Xe-135, Sm-149, U-235 and U-238. Paragraph 3.3 already explained the choice for these isotopes. After each depletion step, the information is extracted from the depletion_results.h5 output file. The evolution of the isotopes for each model will be examined and the inventories of EDEP mode 0 and EDEP mode 3 will be compared.

6.1 Isotopic inventory of EDEP mode 0

Figure 11 shows the evolution of the atom density of the 14 nuclides for EDEP mode 0. This line chart shows the atom density on a logarithmic scale. Figure 12 shows the same atom density on a linear scale. The atom density is shown using both scales to emphasize that the majority of the nuclides only make up for a small percentage in the fuel.

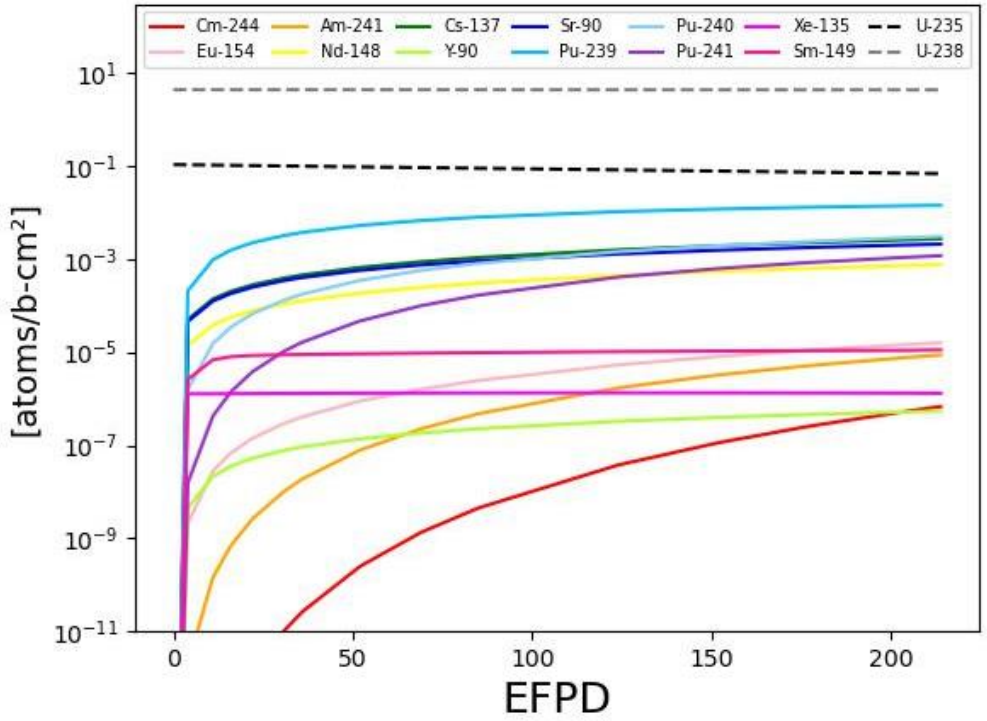

Figure 11: Atom density (log-scale) in function of the EFPD for EDEP mode 0

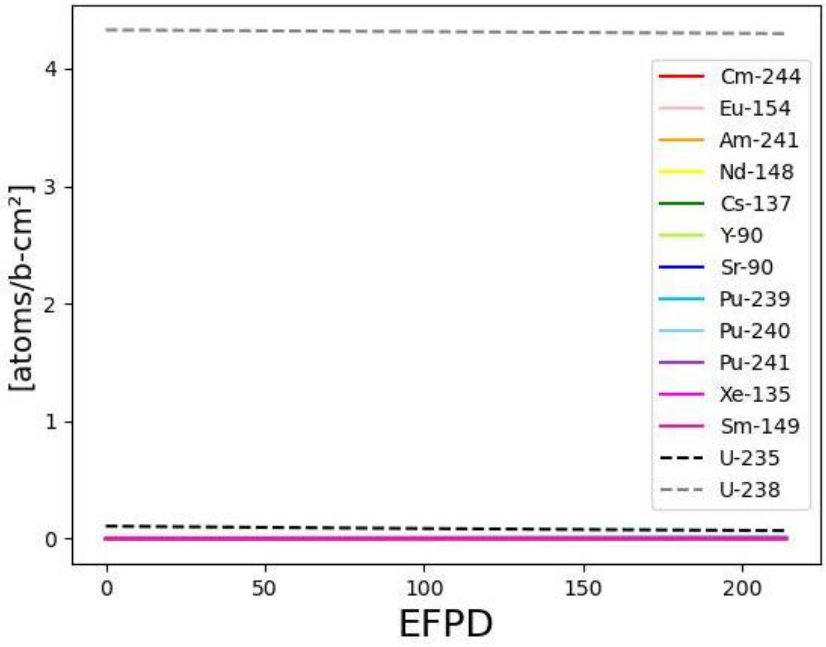

Figure 12: Atom density in function of the EFPD for EDEP mode 0

6.2 Isotopic inventory of EDEP mode 3

Figure 13 and Figure 14 show the evolution of the atom density of the 14 nuclides for EDEP mode 3. Figure 13 plots the atom density on a logarithmic scale while Figure 14 plots the atomic density on a linear scale.

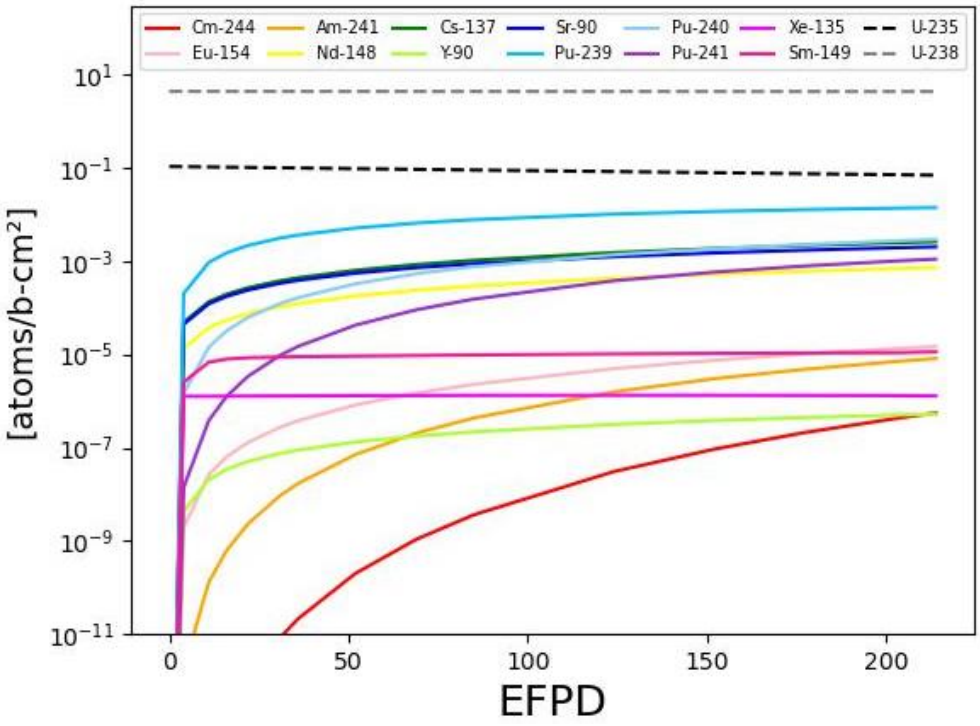

Figure 13: Atom density (log-scale) in function of the EFPD for EDEP mode 3

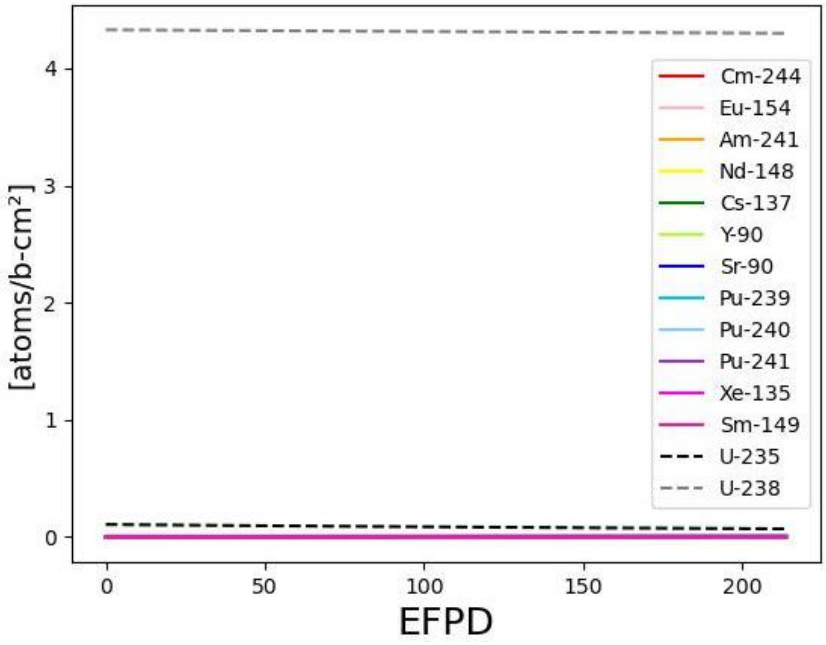

Figure 14: Atom density in function of the EFPD for EDEP mode 0

6.3 Comparison between EDEP mode 0 and EDEP mode 3

The comparison will be made between the isotopic inventories of EDEP mode 0 and EDEP mode 3. For every nuclide, the atom density in function of the EFPD will be compared and plotted together. The relative difference between the values will also be shown. For the calculation of the relative difference EDEP mode 3 is assumed to give the most accurate value. Equation (12) shows the formula used to determine the relative error.

$$RE\ [\%] = \frac{EDEP\ 0 - EDEP\ 3}{EDEP\ 3} * 100\% \qquad (12)$$

6.3.1 Americium-241

Americium-241, short notation Am-241, is an unstable isotope of americium. It is an alpha-emitter and decays to Np-237 with a half-life of 432,6 year. The nuclide Am-241 can be created by radioactive decay of Pu-241 (β^-) and Cm-241 (β^+).

Figure 15 shows the atom density of Am-241 in function of EFPD for both modes. It seems that the values are near each other. Figure 16 however shows the relative difference and there can be concluded that in the early stages of the depletion there is a significant difference of around 11.5%. As the depletion continues, the relative difference decreases and finishes at a value of 6.6%.

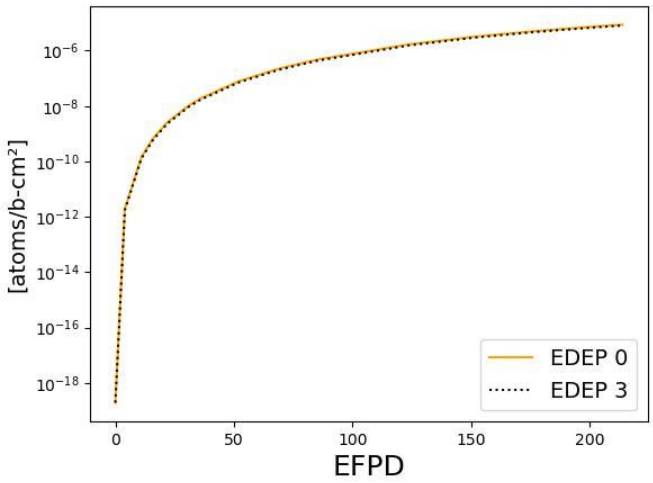

Figure 15: Comparison between atom density of Am-241 in function of EFPD for EDEP mode 0 and EDEP mode 3

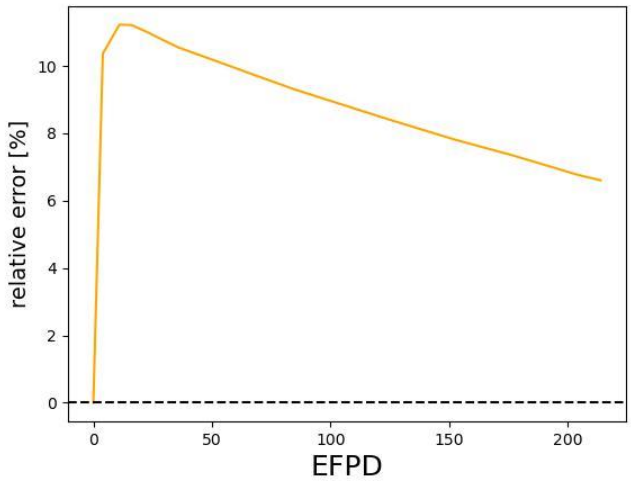

Figure 16: Relative difference between atom density of Am-241 of EDEP mode 0 and EDEP mode 3 in function of EFPD

6.3.2 Curium-244

Curium-244, short notation Cm-244, is an unstable isotope of curium. It is an alpha-emitter and decays to Pu-240 with a half-life of 18.11 year. The nuclide Cm-244 can also undergo spontaneous fission reactions. It is created by a chain of neutron capture and β^--decay starting at U-238. As already explained in 0, Cm-244 is considered a significant neutron emitter in SNF.

Figure 17 shows the atom density of Cm-244 in function of EFPD for both modes. There is a noticeable deviation between the values of EDEP mode 0 and EDEP mode 3. Figure 18 shows the relative difference. It almost immediately peaks at a relative difference of 24.55% and then balances out around a value of 22%. There can be concluded that EDEP mode 0 overestimates the atom density of Cm-244.

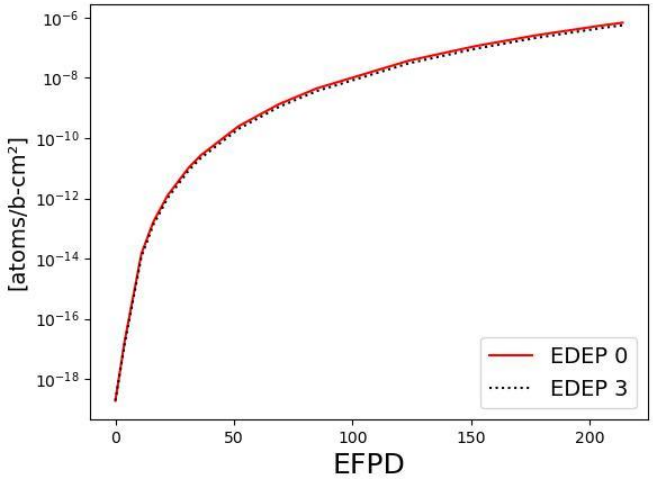

Figure 17: Comparison between atom density of Cm-244 in function of EFPD for EDEP mode 0 and EDEP mode 3

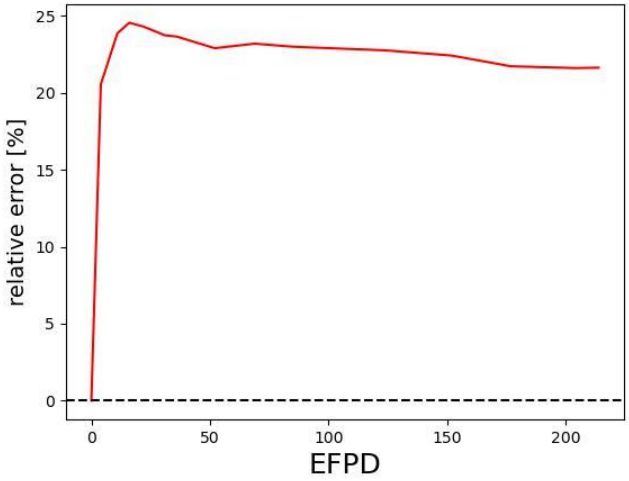

Figure 18: Relative difference between atom density of Cm-244 of EDEP mode 0 and EDEP mode 3 in function of EFPD

6.3.3 Caesium-137

Caesium-137, short notation Cs-137, is an unstable isotope of caesium. It decays to Ba-137 by β- decay with a half-life of 30.08 year. It is a more common fission product of U-235.

Figure 19 shows the atom density of Cs-137 in function of EFPD for both modes. Figure 20 shows the relative difference. The relative difference jumps to 3.5% and steadily increases as the depletion continues. It reaches a value of 3.9%. EDEP mode 0 overestimates the atomic density of Cs-137.

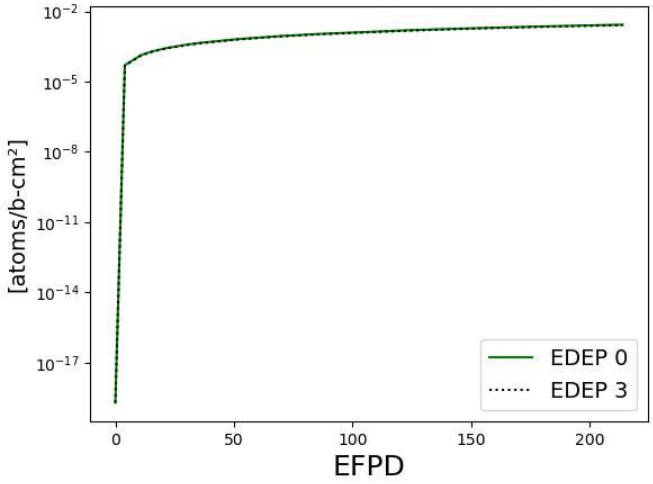

Figure 19: Comparison between atom density of Cs-137 in function of EFPD for EDEP mode 0 and EDEP mode 3

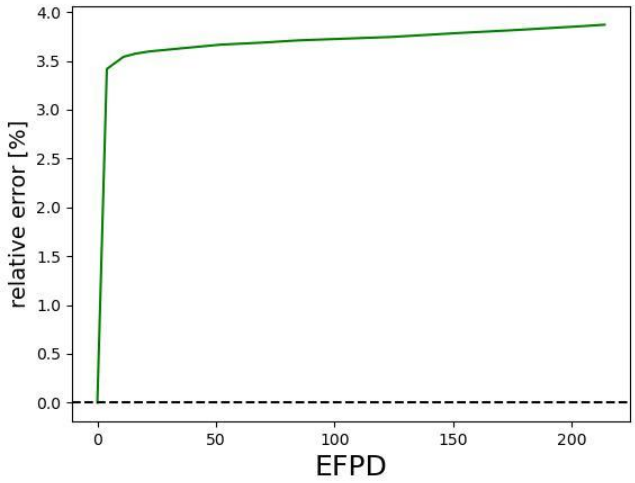

Figure 20: Relative difference between atom density of Cs-137 of EDEP mode 0 and EDEP mode 3 in function of EFPD

6.3.4 Europium-154

Europium-154, short notation Eu-154, is an unstable isotope of europium. It does not occur naturally on Earth. The nuclide Eu-154 decays to Gd-154 by β- decay with a half-life of 8.06 year. A small portion (0.02%) decays by electroncapture to Sm-154. The nuclide Eu-154 is created as a fission product. The importance of Eu-154 in the isotopic inventory lies in its gamma emissions. The most occurring gamma energies are 123 keV (40.79%) and 1274 keV (35.19%).

Figure 21 shows the atom density of Eu-154 in function of EFPD for both modes. Figure 22 shows the relative difference. The increase in the relative difference starts at 7% and reaches 7.7% at the end of the cycle. Once again, EDEP mode 0 overestimates the atomic density.

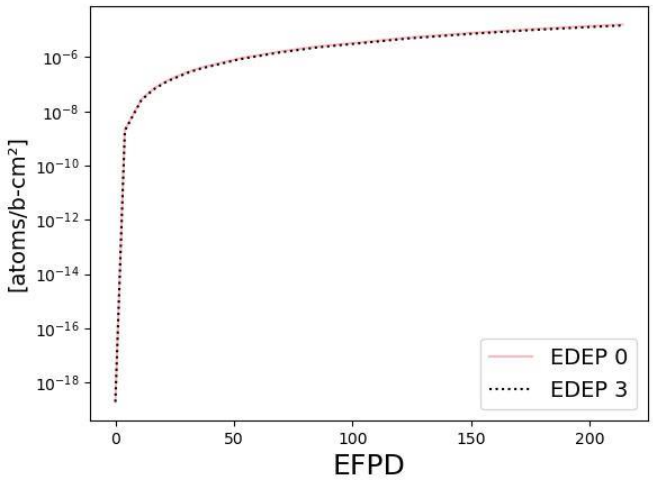

Figure 21: Comparison between atom density of Eu-154 in function of EFPD for EDEP mode 0 and EDEP mode 3

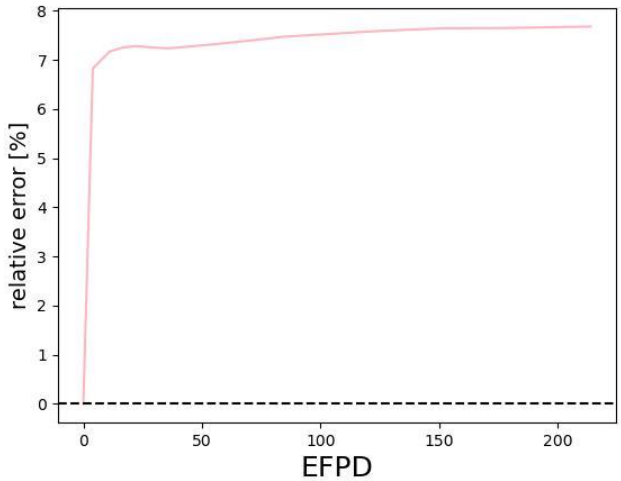

Figure 22: Relative difference between atom density of Eu-154 of EDEP mode 0 and EDEP mode 3 in function of EFPD

6.3.5 Neodymium-148

Neodymium-148, short notation Nd-148, is an technically unstable isotope of europium. As it has a half-life of 3 x 10^{18} year, it is considered stable. The nuclide Nd-148 is created as a fission product. As Nd-148 is created by fissions and does not disappear, it is used as an indicator for burn-up.

Figure 23 shows the atom density of Nd-148 in function of EFPD for both modes. Figure 24 shows the relative difference. The relative difference in the first steps of the depletion is 3.5% and increases until it almost hits 4%. Similar to the previous isotopes, the results from EDEP mode 0 are an overestimation.

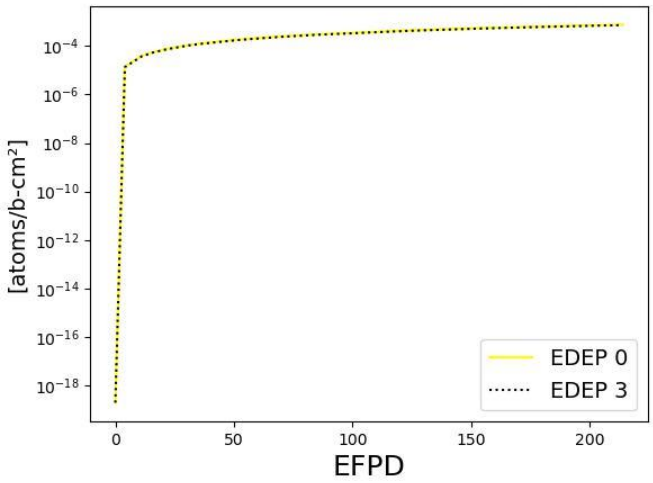

Figure 23: Comparison between atom density of Nd-148 in function of EFPD for EDEP mode 0 and EDEP mode 3

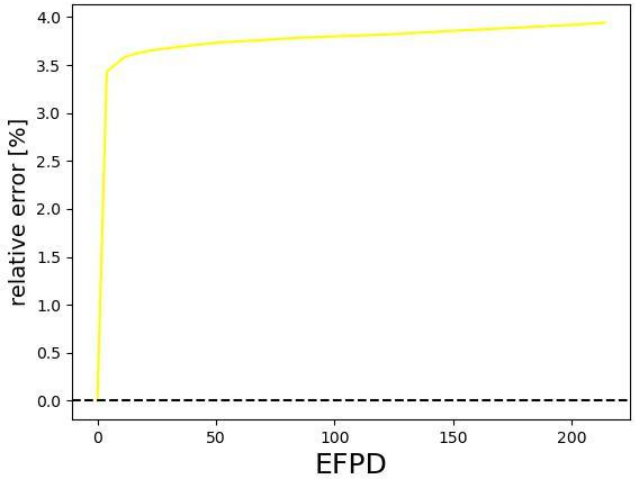

Figure 24: Relative difference between atom density of Nd-148 of EDEP mode 0 and EDEP mode 3 in function of EFPD

6.3.6 Plutonium-239

Plutonium-239, short notation Pu-239, is an unstable isotope of plutonium. The nuclide Pu-239 is an alpha-emitter with a half-life of 24 110 year. It decays to U-235. Pu-239 is formed by neutron capture of U-238, producing U-239, followed by double β^--decay. U-239 is very unstable with a half-life of approximately 23.5 minutes. The nuclide Pu-239 has a neutron fission cross section of 750 barn [17].

Figure 25 shows the atom density of Pu-239 in function of EFPD for both modes. Figure 26 shows the relative difference. The relative difference peaks at 3.4% and gradually decreases when the depletion continues to eventually result in an error of 1.8%. There can be concluded that EFPD mode 0 made an overestimation of the atomic density.

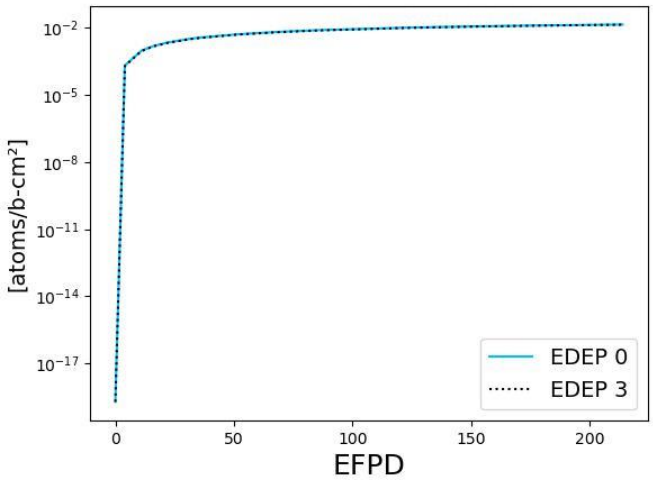

Figure 25: Comparison between atom density of Pu-239 in function of EFPD for EDEP mode 0 and EDEP mode 3

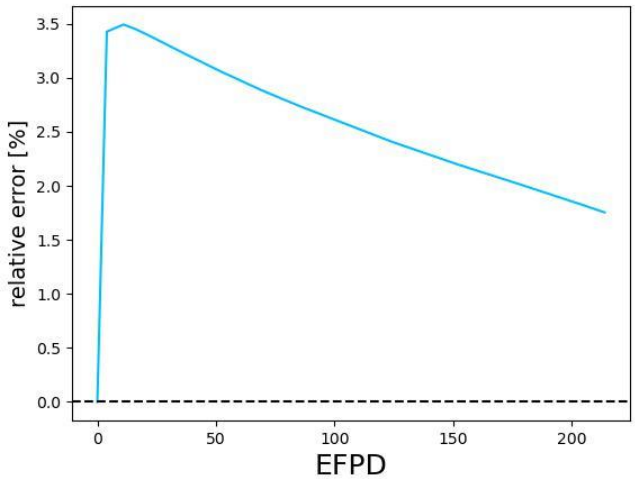

Figure 26: Relative difference between atom density of Pu-239 of EDEP mode 0 and EDEP mode 3 in function of EFPD

6.3.7 Plutonium-240

Plutonium-240, short notation Pu-240, is an unstable isotope of plutonium. It has two important decay modes. On one hand Pu-240 is an alpha-emitter and decays to U-236. On the other hand Pu-240 undergoes spontaneous fission at a small but significant rate. However, Pu-240 has a small neutron fission cross section, 0.059 barn [17]. When Pu-240 captures a neutron, it is more likely that it transmutes to Pu-241 than that it fissions. The nuclide Pu-240 is formed by neutron capture of Pu-239.

Figure 27 shows the atom density of Pu-240 in function of EFPD for both modes. Figure 28 shows the relative difference. The same relative difference pattern is shown as with Pu-239. They are inevitably connected as Pu-240 is created by neutron absorption of Pu-239. The relative error of Pu-240 peaks at 7.2% and plateaus around 5.1%.

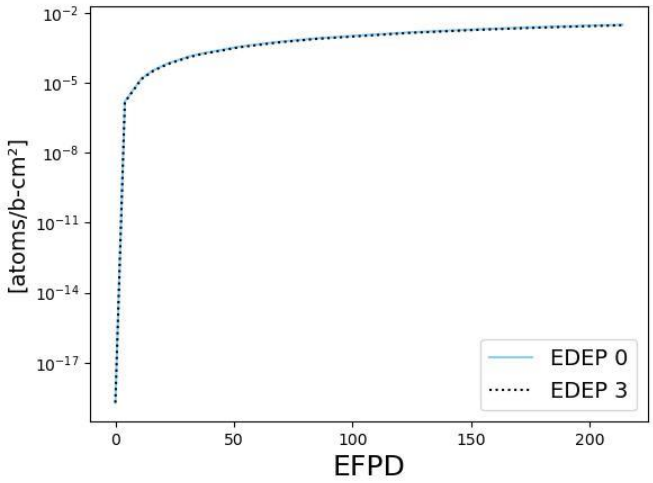

Figure 27: Comparison between atom density of Pu-240 in function of EFPD for EDEP mode 0 and EDEP mode 3

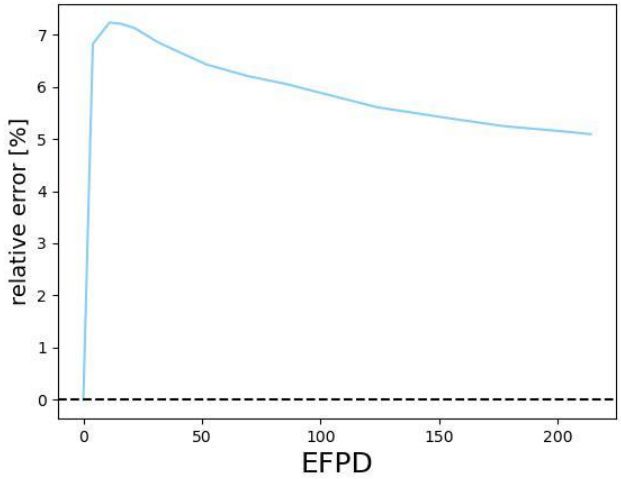

Figure 28: Relative difference between atom density of Pu-240 of EDEP mode 0 and EDEP mode 3 in function of EFPD

6.3.8 Plutonium-241

Plutonium-241, short notation Pu-241, is an unstable isotope of plutonium. it is primarily a β^--emitter and decays to Am-241. It is also able to decay by alpha's to U-237. The half-life is 14.329 year. The nuclide Pu-241 is a fissile isotope with a neutron fission cross section of 1010 barn. It is created by neutron capture of Pu-240, as already mentioned.

Figure 29 shows the atom density of Pu-241 in function of EFPD for both modes. Figure 30 shows the relative difference. It follows the same case as Pu-240. The peak value of the relative error is 11.4% and gradually decreases until it hits 6.8%. As the atomic density of both Pu-239 and Pu-240 was an overestimation for EDEP mode 0, the atomic density of Pu-241 is also an overestimation.

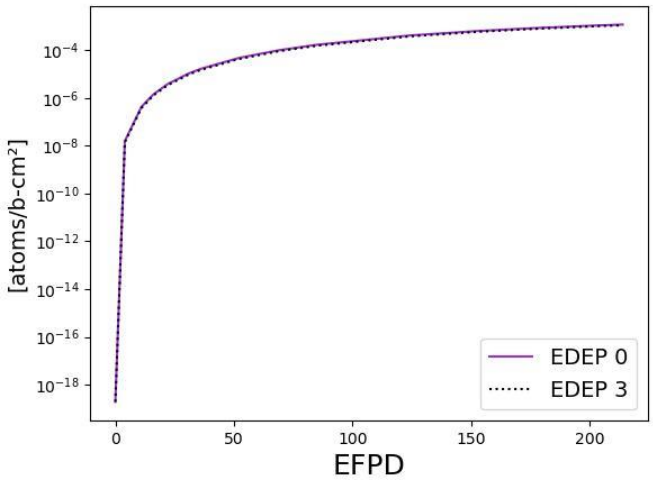

Figure 29: Comparison between atom density of Pu-241 in function of EFPD for EDEP mode 0 and EDEP mode 3

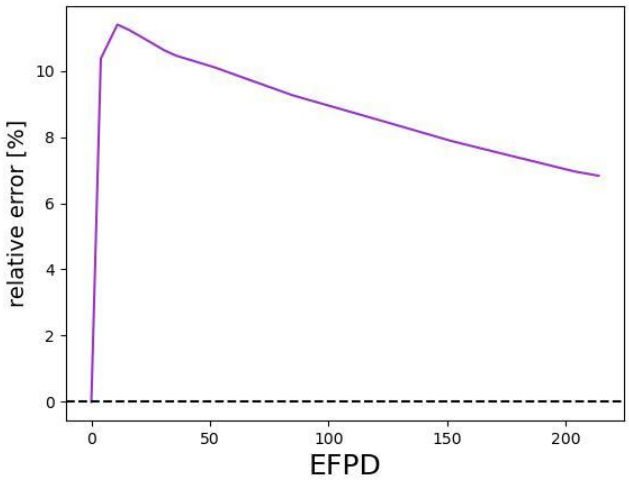

Figure 30: Relative difference between atom density of Pu-241 of EDEP mode 0 and EDEP mode 3 in function of EFPD

6.3.9 Samarium-149

Samarium-149, short notation Sm-149, is a stable isotope of samarium. The nuclide Sm-149 is a neutron poison, meaning that it has a very large neutron absorption cross section, i.e. 40 100 barn [17]. It is created from β^--decay of fission product Nd-149. Nd-149 decays to Pm-149 ($T_{1/2}$ = 1.73 h), which decays to Nd-149 ($T_{1/2}$ = 53.1 h). Since the half-life of Pm-149 is considerably smaller than the half-life of Nd-149, Pm-149 is considered as the fission product. The nuclide Sm-149 disappears when it absorbs a neutron. In normal operation, the atom density of Sm-149 balances out at an equilibrium value. This equilibrium is independent of the neutronflux.

Figure 31 shows the atom density of Sm-149 in function of EFPD for both modes. Figure 32 shows the relative difference. In the first stages of the depletion, the relative difference peaks at 2.3%. At 36 EFPD it briefly touches the 0% mark, before increasing to around 0.4%. At the last depletion step, 214 EFPD, the relative difference jumps to -1.8%. This is the only nuclide with a combination of both positive and negative relative errors.

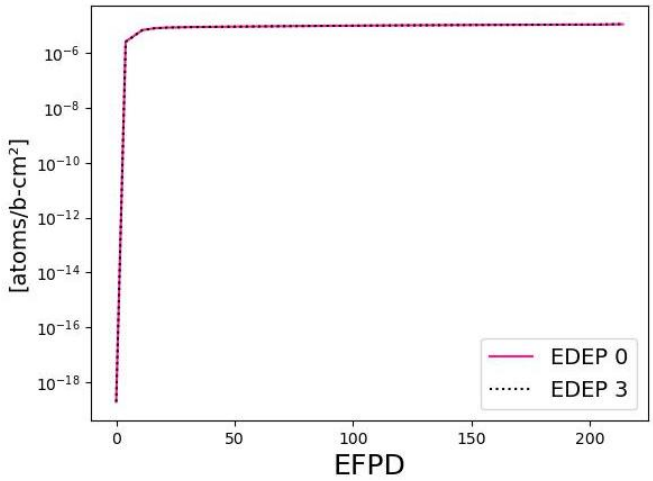

Figure 31: Comparison between atom density of Sm-149 in function of EFPD for EDEP mode 0 and EDEP mode 3

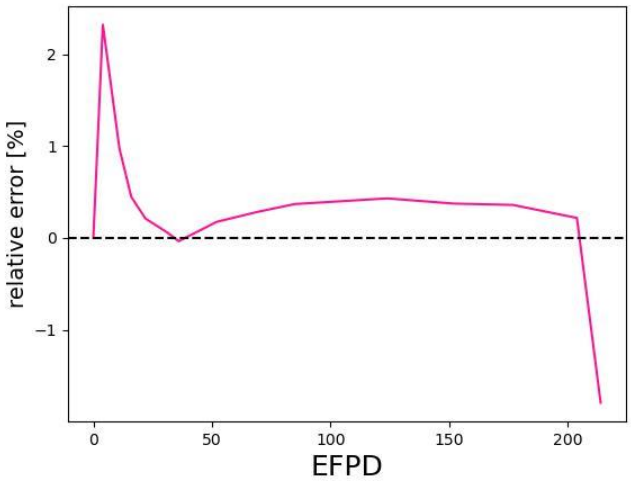

Figure 32: Relative difference between atom density of Sm-149 of EDEP mode 0 and EDEP mode 3 in function of EFPD

6.3.10 Strontium-90

Strontium-90, short notation Sr-90, is an unstable isotope of strontium. It is not naturally occurring on Earth. It is a fission product and decays to Y-90 by β^--decay with a half-life of 28.9 year.

Figure 33 shows the atom density of Sr-90 in function of EFPD for both modes. Figure 34 shows the relative difference. The relative difference starts at 3.5% and starts levelling out at 36 EFPD at a value of around 3.4%. Similar to previous nuclides, the result from EFPD mode 0 is an overestimation.

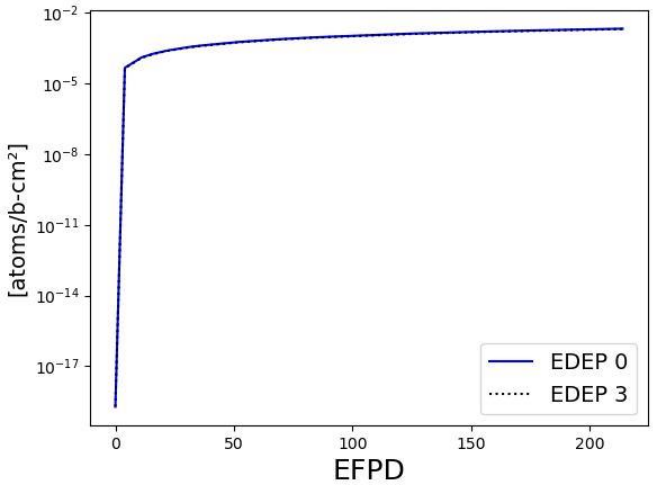

Figure 33: Comparison between atom density of Sr-90 in function of EFPD for EDEP mode 0 and EDEP mode 3

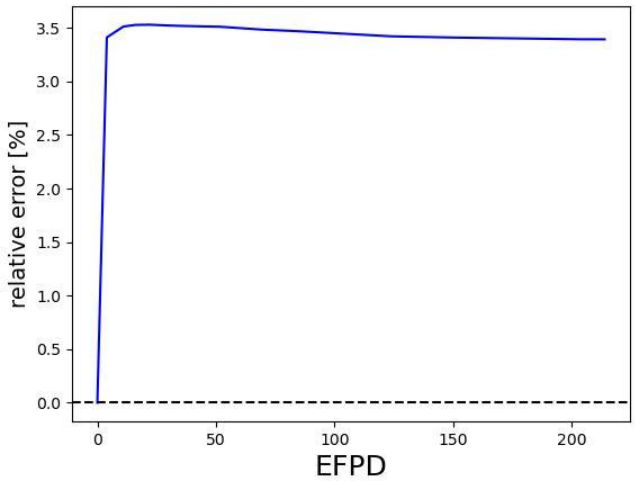

Figure 34: Relative difference between atom density of Sr-90 of EDEP mode 0 and EDEP mode 3 in function of EFPD

6.3.11 Uranium-235

Uranium, short notation U-235, is an unstable isotope of uranium. The nuclide U-235 is a naturally occurring isotope on Earth, but with a relatively low abundance, i.e. 0.72%. Enriched uranium is uranium where the percent composition of U-235 has been increased. This can be done with the process of isotope separation. The enrichments of U-235 that are used in this research are: 1.6%, 2.4% and 3.1%. The nuclide U-235 is present in the original composition of the fuel. It is an alpha-emitter as it decays to Th-231 with a half-life of 7.038 x 10^8 year. Its main use is as a fissile material. The nuclide U-235 has a neutron fission cross section of 586 barn [17].

Figure 35 shows the atom density of U-235 in function of EFPD for both modes. Figure 36 shows the relative difference. The figures clearly show that EDEP mode 0 makes an underestimation of the atomic density of U-235 in the fuel. The relative error steadily decreases until it hits -1.63%

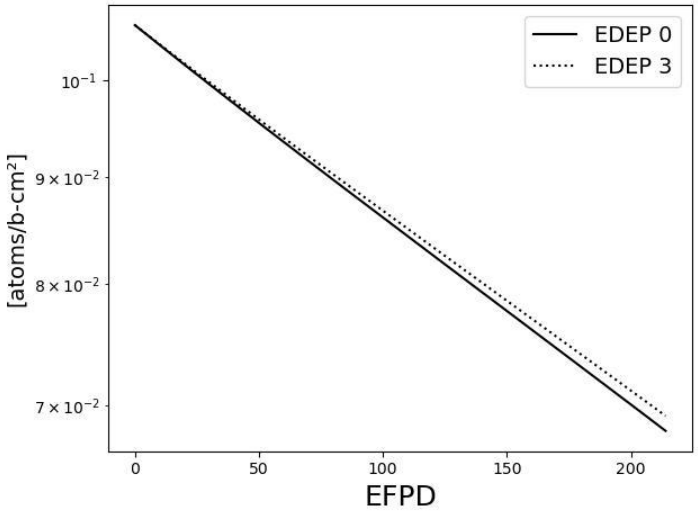

Figure 35: Comparison between atom density of U-235 in function of EFPD for EDEP mode 0 and EDEP mode 3

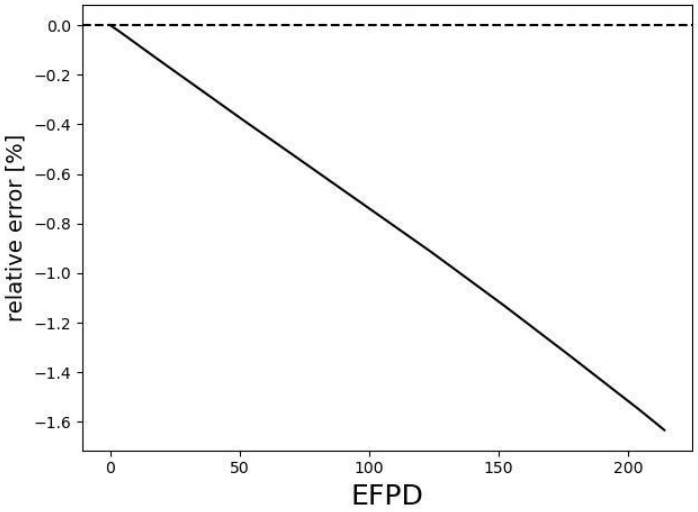

Figure 36: Relative difference between atom density of U-235 of EDEP mode 0 and EDEP mode 3 in function of EFPD

6.3.12 Uranium-238

Uranium-238, short notation U-238, is an unstable isotope of uranium. It is naturally occurring and makes up for 99.27% of natural uranium. The nuclide U-238 undergoes alpha-decay to Th-234 with a half-life of 4.468 x 10^9 year. It is a fertile isotope. Fertile material is not capable of sustaining a nuclear fission chain reaction, but it is able to transmute into fissile material. After neutron capture U-238 transmutes into U-239, which decays to Np-239. Then Np-239 decays to Pu-239, which is fissile material. The nuclide U-238 is originally present in the BEAVRS fuel.

Figure 37 shows the atom density of U-238 in function of EFPD for both modes. Figure 38 shows the relative difference. Similar to U-235, EDEP mode 0 underestimates the atomic density. In contrary to U-235, the final relative difference is only -0.027%.

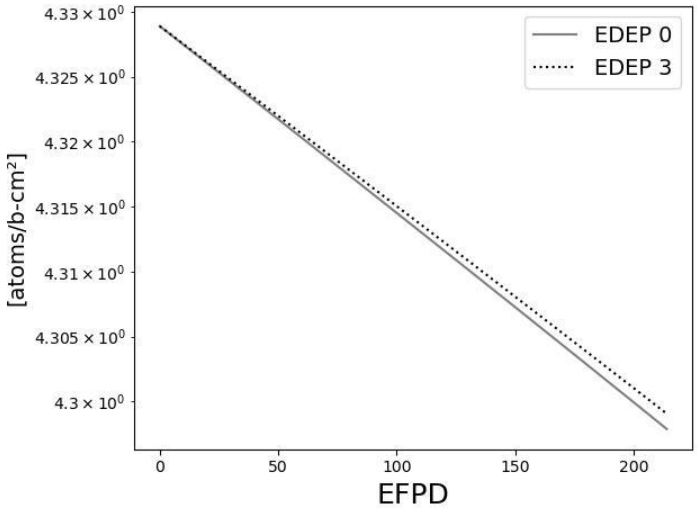

Figure 37: Comparison between atom density of U-238 in function of EFPD for EDEP mode 0 and EDEP mode 3

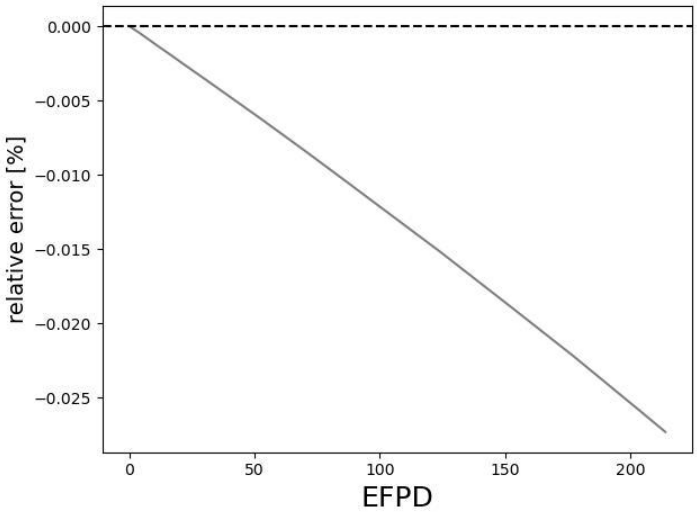

Figure 38: Relative difference between atom density of U-238 of EDEP mode 0 and EDEP mode 3 in function of EFPD

6.3.13 Xenon-135

Xenon-135, short notation Xe-135, is an unstable isotope of xenon. The nuclide Xe-135 is not naturally occurring on Earth and is a fission product of U-235. It can also be created by β-decay of I-135 and I-135 can be obtained from β-decay of Te-135. Both I-135 and Te-135 are fission products. The nuclide Xe-135 decays to Cs-135 with β-decay and a half-life of 9.14 h. Its most important asset is that Xe-135 is the most powerful neutron absorber, with a neutron absorption cross section of 2.65 x 10^6 barn [17]. Similar to Sm-149, Xe-135 will reach an equilibrium level during normal operation. This equilibrium level is dependent of the neutron flux.

Figure 39 shows the atom density of Xe-135 in function of EFPD for both modes. Figure 40 shows the relative difference. The first graph shows that Xe-135 quickly reaches an equilibrium. The second graph shows that the relative error between the two energy deposition modes fluctuates during depletion. Until 152 EFPD the relative error stays around 0.75%, after 152 EFDD is rapidly increases until it hits 1.65%. There can be concluded that EDEP mode 0 overestimates the atomic density of Xe-135.

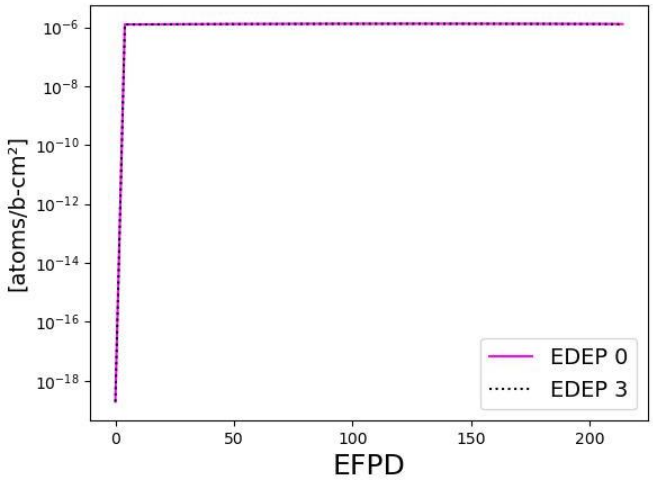

Figure 39: Comparison between atom density of Xe-135 in function of EFPD for EDEP mode 0 and EDEP mode 3

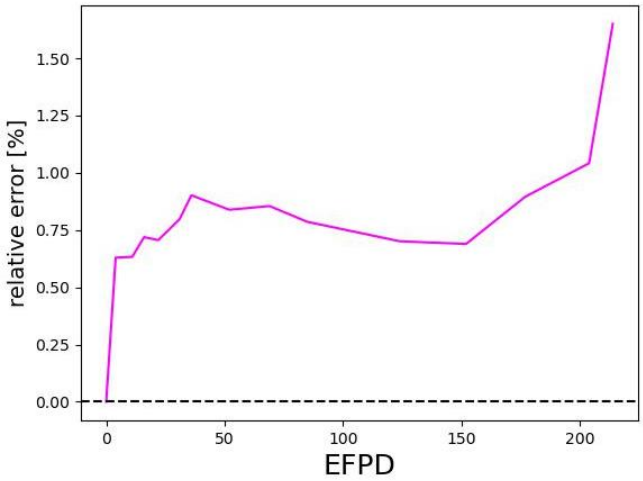

Figure 40: Relative difference between atom density of Xe-135 of EDEP mode 0 and EDEP mode 3 in function of EFPD

6.3.14 Yttrium-90

Yttrium-90, short notation Y-90, is an unstable isotope of yttrium. It is created by β^--decay of Sr-90, with a half-life of 28.90 year. The nuclide Y-90 itself decays to Zr-90 with a half-life of 64.04 h.

Figure 41 shows the atom density of Y-90 in function of EFPD for both modes. Figure 42 shows the relative difference. The evolution of the atomic density is very similar to the evolution of Sr-90. The relative difference starts at 3.4% and levels out around 3.5%. This result of EDEP mode 0 is again an overestimation.

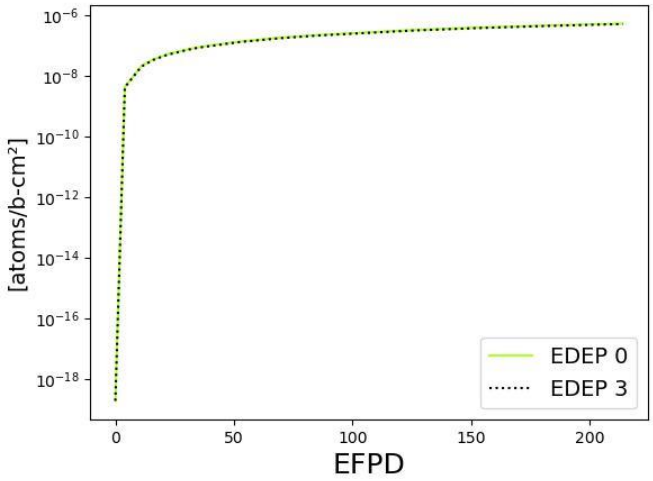

Figure 41: Comparison between atom density of Y-90 in function of EFPD for EDEP mode 0 and EDEP mode 3

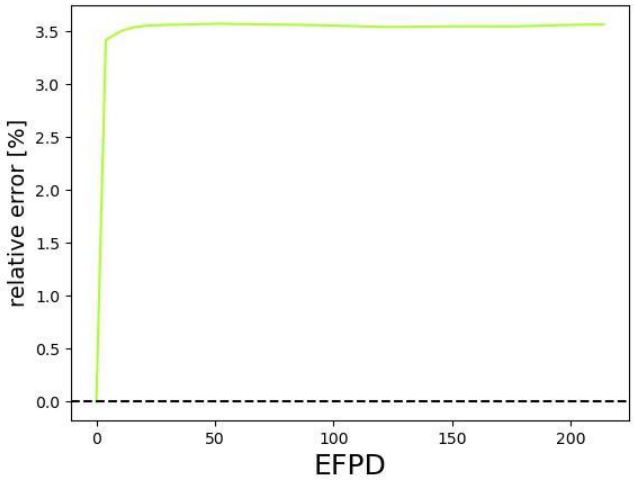

Figure 42: Relative difference between atom density of Y-90 of EDEP mode 0 and EDEP mode 3 in function of EFPD

6.4 Discussion

The previous part compared the atomic densities of the individual isotopes for the two energy deposition models. There can be concluded that for a majority of the isotopes EDEP mode 0 overestimates their atomic density. EDEP mode 0 results only for U-235 and U-238 in a true underestimation. Table 6 shows the relative errors at the final depletion step, sorted from largest absolute value to smallest.

Table 6: Relative errors for isotopic inventory at 214 EFPD

isotope	relative error [%]
Cm-244	21.63
Eu-154	7.68
Pu-241	6.83
Am-241	6.60
Pu-240	5.09
Nd-148	3.94
Cs-137	3.87
Y-90	3.57
Sr-90	3.39
Sm-149	-1.79
Pu-239	1.75
Xe-135	1.65
U-235	-1.63
U-238	-0.03

There is no uncertainty calculated on the isotopic inventory. This is done as it has no added value to the research and it would take a long time to calculate. The isotopic inventory is the solution of a deterministic calculation, the Bateman equation. The Bateman equation, however, has a stochastic input, i.e. the RR. The RR is a mean and random variable, but due to the central limit theorem, it is normally distributed and therefore its uncertainty can be easily determined. To obtain an uncertainty on the isotopic inventory, the process of simulating a transport calculation and solving the Bateman equation needs to be repeated multiple times. As previously mentioned, the uncertainty scales with the number of histories ($\frac{1}{\sqrt{N}}$), so the whole process would have to be repeated for at least 30 times. The primary aim of this research is to use the same statistics, but different models, to see if there is any bias in the models.

As EDEP mode 0 overestimates the energy deposited locally in the fuel, it overestimates the power in the fuel and therefore the normalisation factor. This results in an overestimation of the RR. This leads to an increased burn-up rate of the fuel, i.e. U-235 and U-238. This is why there is an underestimation of the atomic densities of U-235 and U-238. In EDEP mode 0, more U-235 atoms are already burned because of the higher RR. This leads to an increase in fission products and actinides.

These increments and reductions result in safety issues of SNF. If there is more fissile material than expected, this can cause the SNF to become critical during transport. An overestimation of neutron absorbers present in the SNF can also cause criticality to occur. On the other hand, an overestimation of important γ-emitters and neutron emitters like Eu-154 and Cm-244 lead to higher safety measures than required. Overestimations of important decay heat isotopes, e.g. Sr-90, Y-90, Cs-137, Am-241 and Cm-244, can also lead to higher safety measures.

It can be concluded that there is a significant difference between the isotopic inventories of both energy deposition models. While there will be both increments and reductions of safety, assessing the isotopic inventory inaccurately will lead to problems with transport, storage, disposal and assembly shuffling for next cycles. The problems may involve safety, but are also economic and ecological.

7 Fission parameters

In this chapter the results from the tallies are described. As already explained, a tally uses filters to pick a region of the phase space to score in. Two filters were used, e.g. the material filter and the particle filter. Fuel 7 and fuel 97 were chosen with the material filter. These are materials present in the fuel of assembly 7 and assembly 97. As particles neutrons, photons, electrons and positrons were selected. The scores were flux, fission rate, heating-local and heating. Heating-local assumes that the energy from photons is deposited locally while heating assumes that it is not deposited locally.

The results from tallies are not yet normalised, meaning that all tally scores are units per source particle simulated. To convert the tally scores in a more natural unit, normalisation is needed. For a k-eigenvalue calculation, the volume and the power is used to perform the normalisation. First, the normalisation factor needs to be determined. First, a tally of the heating score (H) over the entire system needs to be performed and then the heating rate needs to be calculated. This is demonstrated by Eq. (13).

$$H' = 1.602 * 10^{-19} \left[\frac{J}{eV}\right] * H \, [\frac{eV}{source}]$$

(13)

The normalisation factor is obtained by dividing the power by the observed heating rate. Equation (14) shows the formula for the normalisation factor.

$$f = \frac{P}{H'} = \left[\frac{J/s}{J/source}\right] = [\frac{source}{s}]$$

(14)

To obtain a score in typical units, the scores needs to be multiplied by the normalisation factor and divided by the relevant volume. Normalisation is not performed on these results as it has no added value to the research. The first reason is that the tally of the heating score over the whole core would be time-consuming. This is also why it was decided to only inspect two assemblies, since tallying the whole core would take a long time. Normalisation can also be performed using the heating score and the power of only the researched assembly. This is not an option as the power in one assembly is not known and there is no tally to calculate it. As this thesis wants to inspect whether the different energy deposition models have a bias on the observables of interest and only the relative difference is determined, normalising the score results has no added value.

7.1 Assembly 7

7.1.1 Neutrons

Figure 43 shows the neutron flux and neutron fission rate in function of EFPD for the top right assembly. Figure 44 demonstrates the heating-local and heating scores. As the neutron flux and neutron fission rate are inevitably linked, the graphs follow the same evolution. The further the depletion progresses, the higher the deviation is between EDEP mode 0 and EDEP mode 3. The difference between the modes becomes extremely significant at the last stages of the simulation.

As seen in Figure 43: Neutron flux (left) and neutron fission rate (right) in function of EFPD for A7, EDEP mode 3 is more capable of keeping the neutron flux around the same level. If the neutron flux stays more or less the same, the criticality of the core is better preserved. The spiky behaviour is due to the change of the boron concentration each time-step.

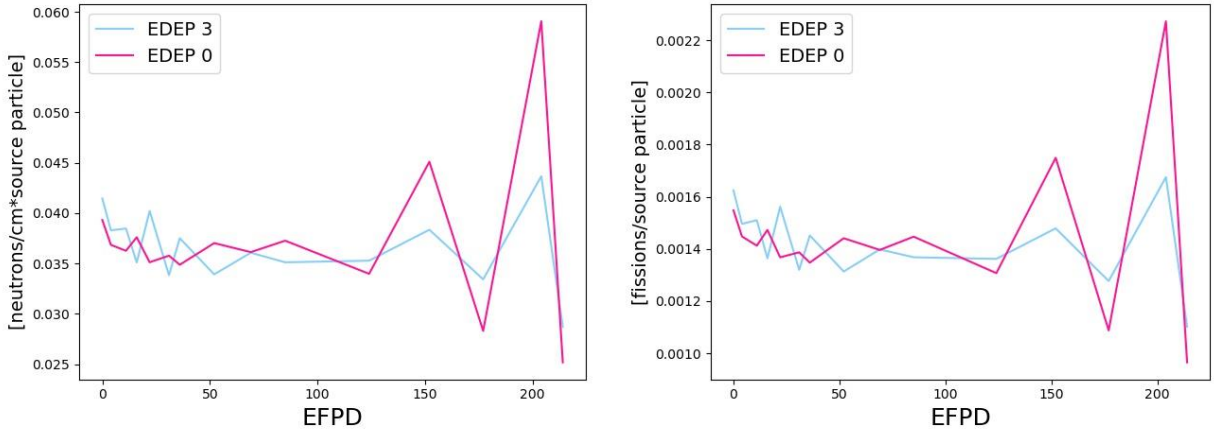

Figure 43: Neutron flux (left) and neutron fission rate (right) in function of EFPD for A7

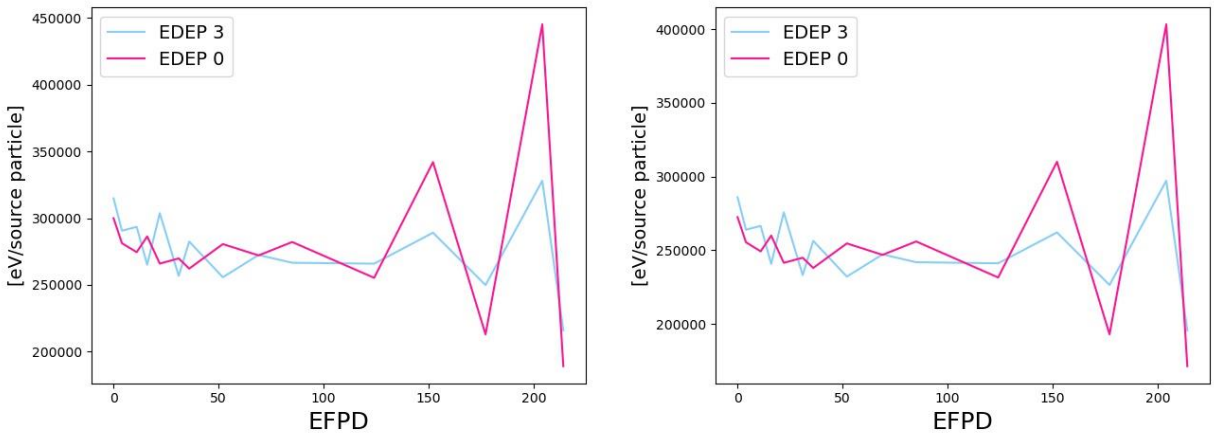

Figure 44: Neutron heating-local (left) and neutron heating (right) in function of EFPD for A7

As seen in Figure 45, the relative difference for the neutron flux peaks at more than 30% at the end of the depletion. There is a pattern of a positive and negative difference each depletion time-step. The difference increases each time-step and leaps upwards during the final steps.

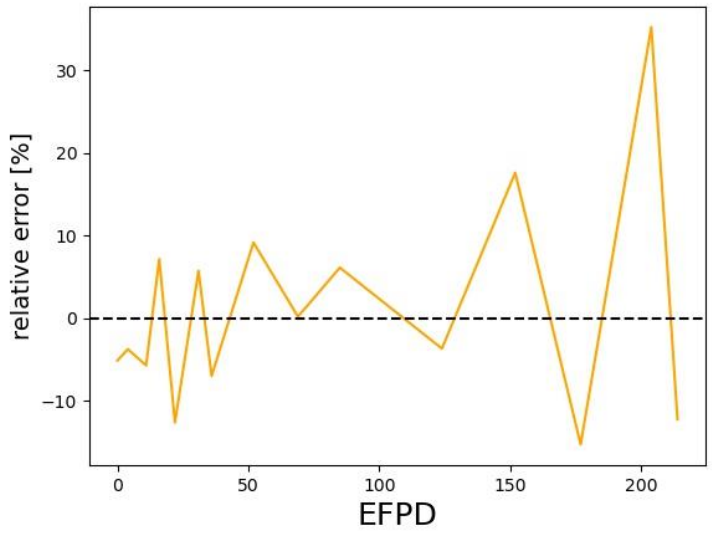

Figure 45: Relative error between neutron flux of EDEP 0 and EDEP 3 for A7

7.1.2 Photons

Figure 46 shows the results of the photon scores, e.g. flux and heating. The flux and heating follow the same pattern. The photon heating is significantly lower than the neutron heating, with heating values of 1000 eV/source particle in contrary to 250 000 eV/source particle for neutrons.

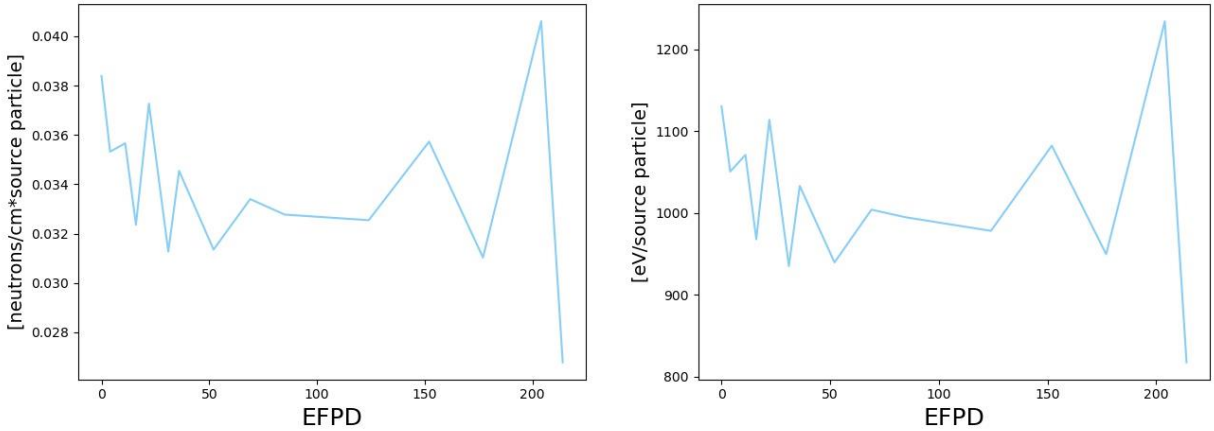

Figure 46: Photon flux (left) and photon heating (right) in function of EFPD for A7

7.1.3 Electrons and positrons

As Figure 47 shows, the electron heating follows the same pattern as the photons, while the positrons are completely independent. The heating values for electrons are more significant than those of the photons, with a value of around 20 000 eV/source particle. The positron heating however is negative. This is caused by the way of how thick-target bremsstrahlung (TTB) is modelled in OpenMC. Photon energies are randomly sampled between 0 and the energy of the electron or positron. When multiple photons are created from TTB, the total photon energy can exceed the original energy of the electron/positron. If the positron heating is negative, this means that too much energy was given to the photons and the positron heating is used to correct this.

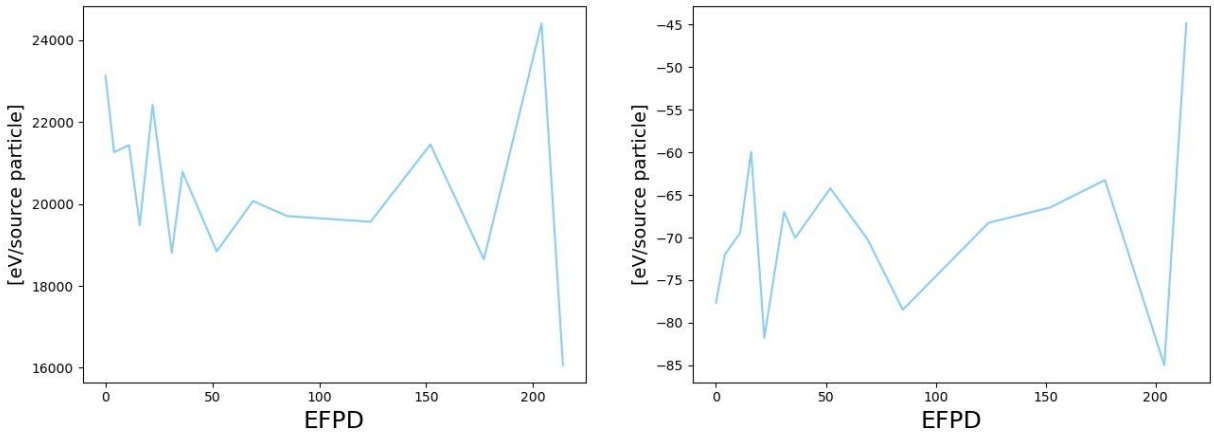

Figure 47: Electron heating (left) and positron heating (right) in function of EFPD for A7

7.1.4 Total heating

Figure 48 plots the different particle induced heating in function of EFDP. The particle induced heating of EDEP mode 3 are plotted together with the neutron heating-local of EDEP mode 0. The most important contributor to the heat is the neutron heating, followed by electron heating.

Figure 49 shows the summed heating of all particles for both modes. The summed heating of EDEP mode 3 is not the same as heating-local of EDEP mode 0. Conservation of energy does occur in nuclear fuel but the difference in energies lies in the normalisation. The modes would have a different normalisation factor. It is expected that after normalisation, the heating-local of EDEP mode 0 would be the same as the summed heating of the particles.

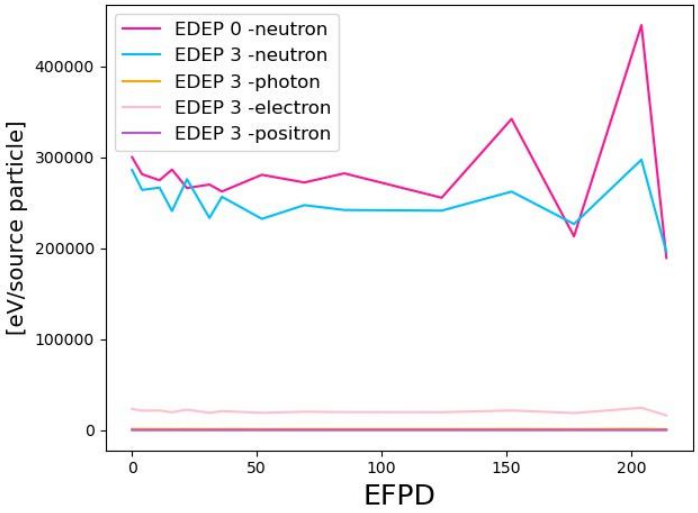

Figure 48: Particle heating in function of EFPD for A7

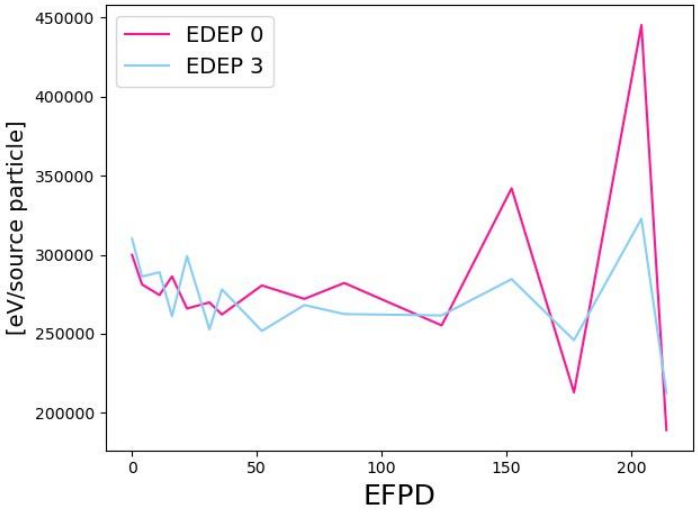

Figure 49: Summed particle heating in function of EFPD for A7

7.2 Assembly 97

7.2.1 Neutrons

Figure 50 shows the neutron flux and neutron fission rate in function of EFPD for the central assembly. Figure 51 demonstrates the heating-local and heating scores. The four graphs follow the same trend, but the deviation between EDEP mode 0 and EDEP mode 3 is less significant than for A7. This is caused by the fact that the spatial distribution of the flux is not uniform in the whole core.

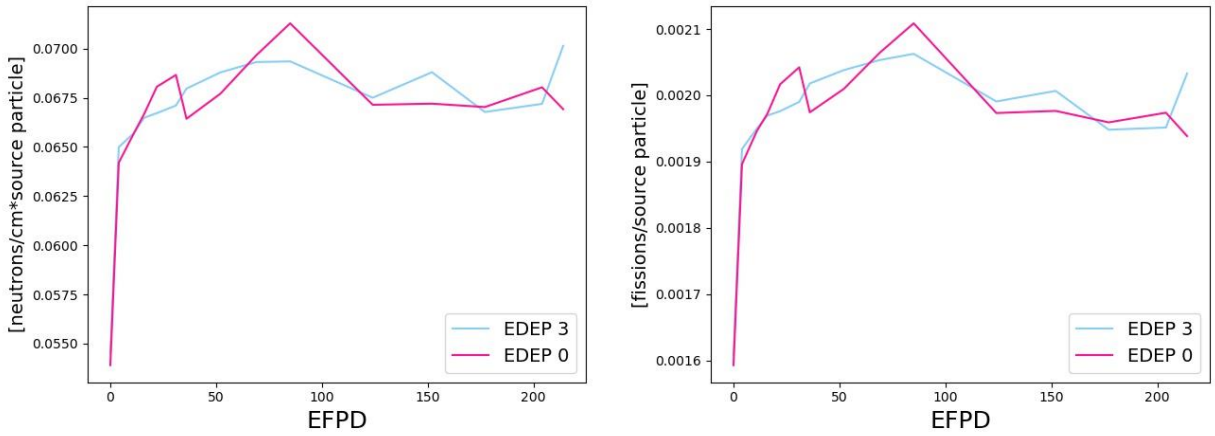

Figure 50: Neutron flux (left) and neutron fission rate (right) in function of EFPD for A97

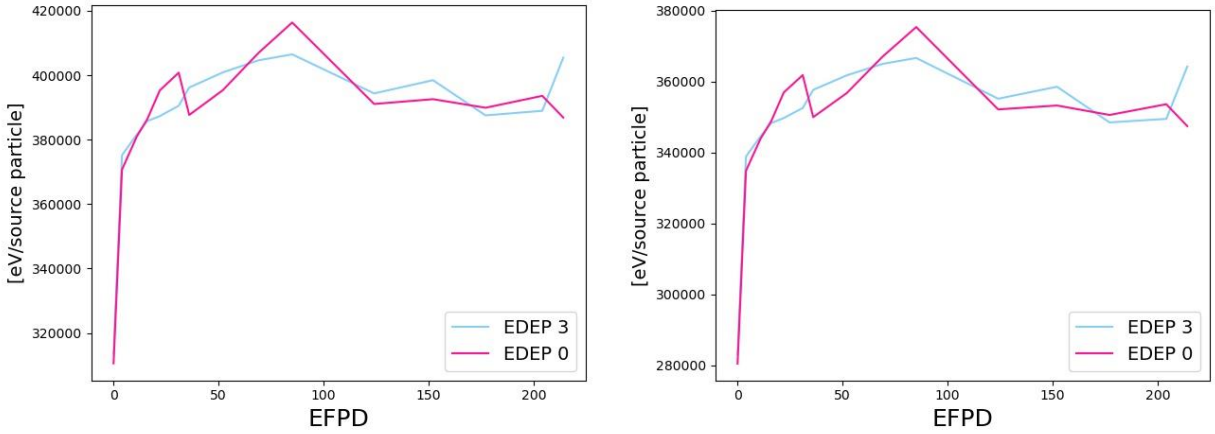

Figure 51: Neutron heating-local (left) and neutron heating (right) in function of EFPD for A97

Figure 52 shows the relative difference for the neutron flux in function of EFPD. The relative difference is less significant for A97 than for A7. The pattern of an alternating negative and positive value is also occurring in A97. The relative difference has a maximal value of +3% or -4.5%.

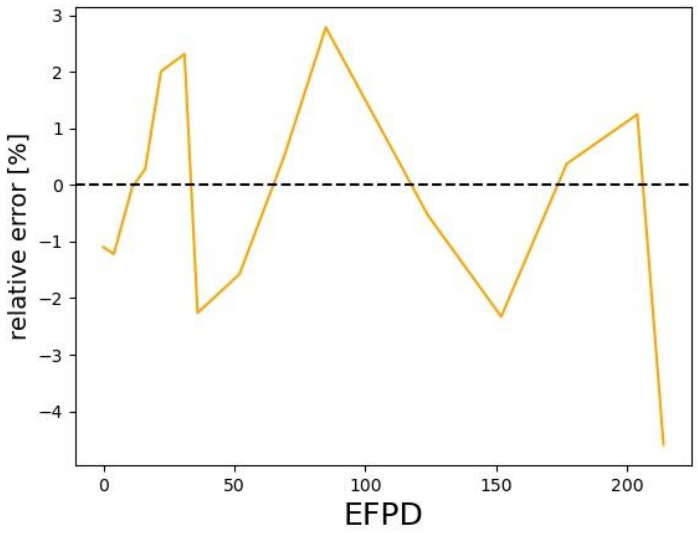

Figure 52: Relative error between neutron flux of EDEP 0 and EDEP 3 for A97

7.2.2 Photons

Figure 53 shows the results of the photon scores, e.g. flux and heating. The flux and heating follow the same pattern. The same case as A7 is seen here, the photon heating is significantly lower than the neutron heating. Photon heating averages at a value of 1700 eV/source particle, while neutron heating averages at a heating of 360 000 eV/source particle.

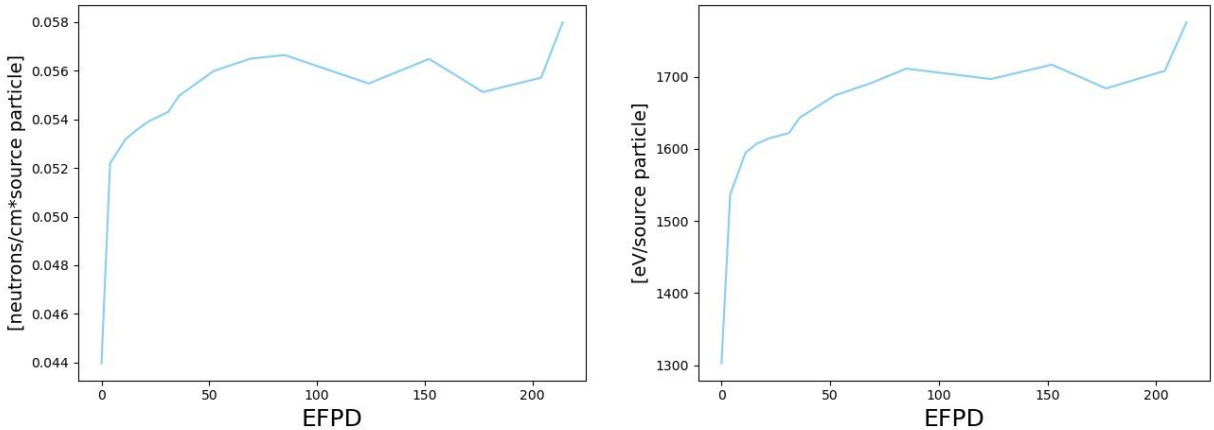

Figure 53: Photon flux (left) and photon heating (right) in function of EFPD for A97

7.2.3 Electrons and positrons

As Figure 54 shows, the electron heating follows the same pattern as the photons, while the positrons are completely independent. The same trend is seen here, as the electron heating is more significant than the photon heating, but less than the neutron heating. The positron heating is again negative.

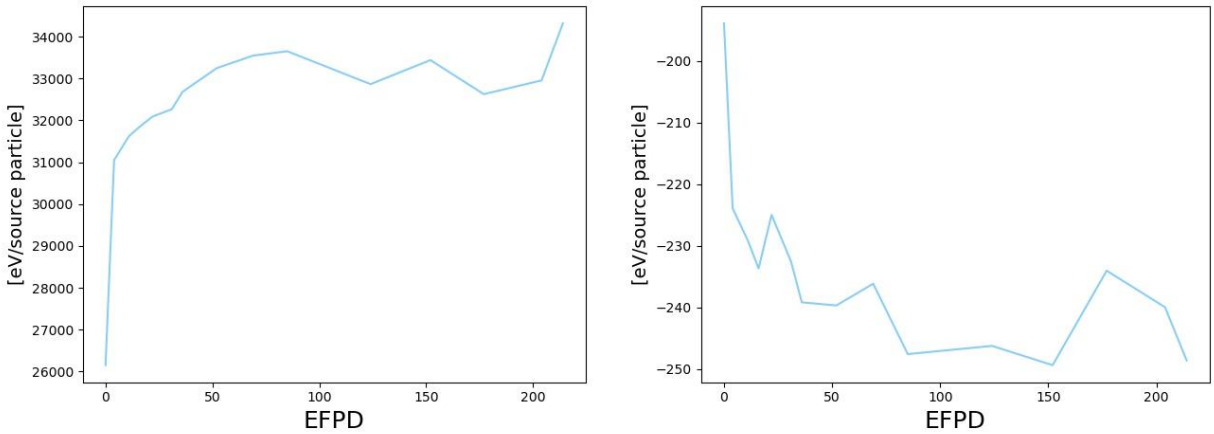

Figure 54: Electron heating (left) and positron heating (right) in function of EFPD for A97

7.2.4 Total heating

Figure 55 plots the different particle heatings in function of EFDP. The particle heatings of EDEP mode 3 are plotted together with the neutron heating-local of EDEP mode 0. The most important contributor to the heat is the neutron heating, followed by electron heating.

Figure 56 shows the summed heating of all particles for both modes. The summed heating of EDEP mode 3 is not the same as heating-local of EDEP mode 0. This again is caused by not-normalisation.

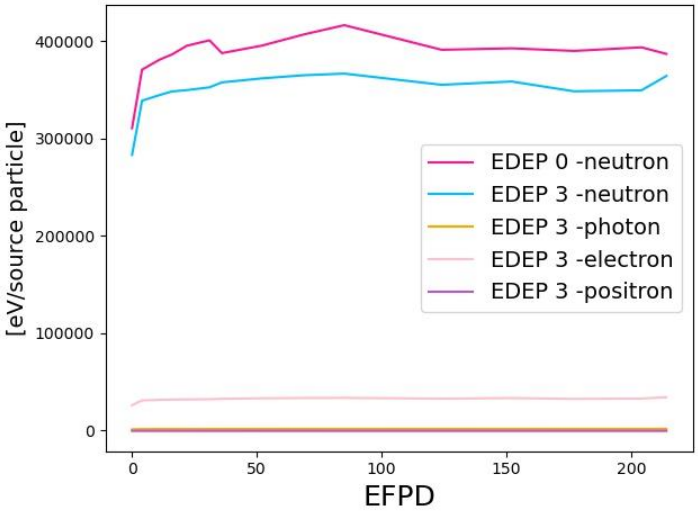

Figure 55: Particle heating in function of EFPD for A97

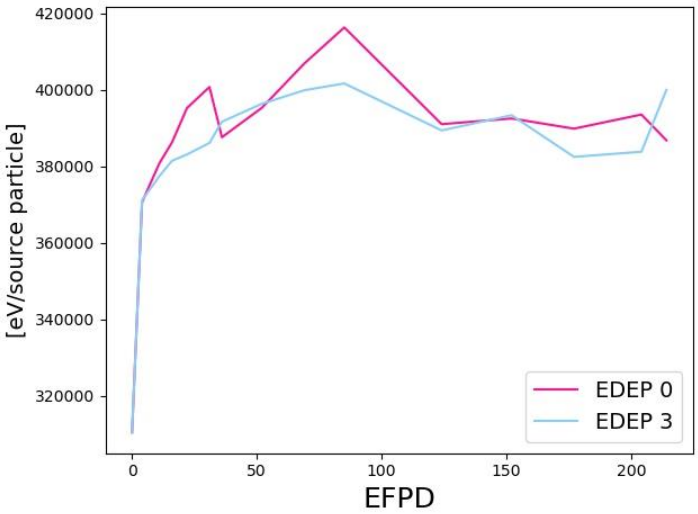

Figure 56: Summed particle heating in function of EFPD for A97

8 Conclusion

The aim of this thesis is to inspect whether the different energy deposition models have an influence on the observables of interest. The two energy deposition models that were studied were EDEP mode 0 and EDEP mode 3. EDEP mode 0 assumes that all energy is deposited locally in the fuel. EDEP mode 3 assumes that photons deposit their energy at the end of their track and that neutrons undergo reactions along their track outside the fuel. EDEP mode 3 causes a redistribution of the energy of EDEP mode 0.

The three observables that were observed are the critical boron concentration, the isotopic inventory and the fission parameters. These three are inevitably linked. It can be concluded that the different energy deposition models do have a significant effect on the observables. If one assumes that the energy is solely deposited locally, the power in the fuel is overestimated. This leads to an overestimation of the reaction rate and an overestimation of the burn-up rate. This results in an underestimation of the atomic densities of U-235, U-238 and Sm-149 and an overestimation of the atomic densities of the other fission products and actinides. Because of the lower estimated atom density of U-235 and overestimated atom density of Xe-135, the criticality of the core is underestimated. This results in a lower critical boron concentration. The fission parameter results show that the effect of different energy deposition models is more significant near the edge of the core. This is caused by the non-uniformity of the spatial distribution of the neutron flux in the core.

At the end of the first cycle the relative difference between the two models is up to 25% for the isotopic inventory and almost 100% for the critical boron concentration. The relative difference for the fission parameters depends on the location of the assembly. The difference for the central assembly is less significant than the difference for an assembly near the edge of the core. The maximal relative difference is respectively +35% and -4.5%. This deviation from the assumed more accurate value, e.g. the results from EDEP mode 3, can cause severe problems when the data is used for further applications. The isotopic inventory is important for transport, storage and disposal of the SNF. If the criticality of the SNF is underestimated, a chain reaction can occur when not wanted. This can cause severe safety problems. The criticality of the SNF can be underestimated by underestimating the atomic density of U-235 or overestimating the atomic density of the neutron poisons. The overestimation of certain fission products and actinides can lead to more extensive safety precautions than needed. The isotopic inventory is also important for the reshuffling of the core for the following cycles. If the isotopic inventory is not accurate, this can cause criticality problems and can have severe consequences. The atom density of U-235 is underestimated and the atom density of Xe-135 is overestimated at the end of the cycle, this means that the core has a higher chance to gain criticality than expected with the results from EDEP mode 0.

The results show that EDEP mode 3 is more accurate and that less accurate results can cause possible safety issues. The number one disadvantage of EDEP mode 3 is the simulation time. The total depletion simulation time is 3.5 times higher than the total simulation time of EDEP mode 0.

This research was merely the first step to a conclusion on the influence of energy deposition models on observables of interest in Monte Carlo codes. Future research consists of continuing with BEAVRS and modelling and simulating next cycles. Cycle 2 is described in the BEAVRS document [7] and includes a reshuffled core with fuel from cycle 1, but also fresh UO_2 fuel with enrichments of 3.2% and 3.4%. In addition to reshuffling, the position of the burnable absorber rods changes. The position of the instrument tubes, control rod and shutdown banks stays the same. The level of burn-up is still

relatively low after two cycles, so more cycles should be constructed and simulated to obtain an estimate of the difference of the isotopic inventory at discharge burn-up between different energy deposition models. These cycles should be simulated and at the end the same observables would be determined and evaluated. This will lead to a conclusion whether the difference between the energy deposition models will increase or balance out.

Bibliography

[1] X Monte Carlo Team, Los Alamos, "MCNPX "MCNPX 2.4.0. Monte Carlo N-Particle Transport Code System for Multiparticle and High Energy Applications," CCC-715, LA-CP-02-408, 2002.

[2] J. Leppänen, "The Serpent Monte Carlo code: Status, development and applications in 2013.," *Annals of Nuclear energy,* vol. 82, pp. 142-150, 2015.

[3] Los Alamos National Laboratory, "The Monte Carlo Method and MCNP –A Brief Review of Our 40 Year History," in *Industrial Radiation and Radioisotope Measurement Applications*, Chicago, 2017.

[4] "A General Monte Carlo N-Particle (MCNP) Transport Code," Los Alamos National Laboratory, [Online]. Available: https://mcnp.lanl.gov/. [Accessed 15 April 2022].

[5] J. Leppänen, "Greetings from the Serpent developer team & current status and future plans for Serpent 2," in *International Serpent UGM*, Espoo, 2018.

[6] P. K. Romano and B. Forget, "The OpenMC Monte Carlo particle transport code," *Annals of Nuclear Energy,* vol. 51, pp. 274-281, 2013.

[7] N. Horelik, B. Herman, B. Forget and K. Smith, "Benchmark for Evaluation and Validation of Reactor Simulations (BEAVRS)," Sun Valley, 2020.

[8] Computational Reactor Physics Group, "CRPG - BEAVRS," Massachusetts Institute of Technology, [Online]. Available: https://crpg.mit.edu/research/beavrs. [Accessed 27 March 2022].

[9] G. Van den Eynde, Reactorfysica, UHasselt, 2021-2022.

[10] W. Haeck, "An Optimum Approach to Monte Carlo Burn-up," 2007.

[11] F. M. Dekking, C. Kraaikamp, H. P. Lopuhaa and L. E. Meester, A Modern Introduction to Probability and Statistics, New York: Springer London Ltd, 2007.

[12] M. Pusa, "Higher-Order Chebyshev Rational Approximation Method and Application to Burnup Equations," *Nuclear science and engineering: the journal of the American Nuclear Society,* vol. 182, 2016.

[13] R. Tuominen, V. Valtavirta and J. Leppänen, "New energy deposition treatment in the Serpent 2 Monte Carlo transport code," *Annals Of Nuclear Energy,* vol. 129, pp. 224-232, 2019.

[14] "OpenMC," [Online]. Available: https://openmc.org/. [Accessed 11 May 2022].

[15] VSC, "VSC - about," [Online]. Available: https://www.vscentrum.be/about. [Accessed 11 May 2022].

[16] VSC, “VSC - offer,” [Online]. Available: https://www.vscentrum.be/offer. [Accessed 11 May 2022].

[17] J. Magill, R. Dreher and Z. Sóti, Karlsruher Nuklidkarte, 10. Edition, 2018.

[18] Joint Research Centre (JRC), “Observables of interest for the characterisation of Spent Nuclear Fuel,” Luxembourg: Publications Office of the European Union, Geel, 2018.

[19] A. L. Lund and P. K. Romano, “Implementation and Validation of Photon Transport in OpenMC,” National Technical Information Service, Alexandria, 2018.

[20] P. K. Romano, C. J. Josey, A. E. Johnson and J. Liang, “Depletion capabilities in the OpenMC Monte Carlo particle transport code,” *Annals of Nuclear Energy,* vol. 152, art. 107989, 2021.